12-20-2009

Polarizing Optical Devices Based on Embedded One-Dimensional Subwavelength-Structured Photonic-Crystal Layers

Hazem Khanfar
University of New Orleans

Polarizing Optical Devices Based on Embedded One-Dimensional Subwavelength-Structured Photonic-Crystal Layers

A Dissertation

Submitted to the Graduate Faculty of the
University of New Orleans
in partial fulfillment of the
requirements for the degree of

Doctor of Philosophy
in
Engineering and Applied Science
Electrical Engineering

by

Hazem Khuloqi Khanfar

B.Sc. Alquds University, 2001
M.Sc. Jordan University of Science and Technology, 2003

December 2009

Dedication

To my parents, my wife, and my children Ahmed and Sarah.

Acknowledgments

I would like to express my sincere gratitude to my major professor Dr. Rasheed Azzam for his support, guidance and encouragement. My special thanks to the dissertation committee members, Dr. Dimitrios Charalampidis, Dr. Ashok Puri, Dr. George Ioup, and Dr. Juliette Ioup, for their valuable suggestion and for their careful reading of this work.

Contents

List of Figures

List of Tables

Abstract

Quarter-wave retarders (QWR) that employ total internal reflection (TIR) and interference of light in a transparent thin-film coating at the base of a prism are presented. Explicit equations that guide the optimal design are provided. The optimal refractive index and normalized thickness of QWR coatings on glass and ZnS prisms are determined as functions of the internal angle of incidence from 45^o to 75^o. An achromatic QWR that uses an Si_3N_4-coated N-BK10-Schott glass prism is also presented with retardance error of $< 3^o$ over the 400-600 nm wavelength range.

An iterative procedure for the design of a polarizing beam splitter (PBS) that uses a form-birefringent, subwavelength-structured, one-dimensional photonic-crystal layer (SWS 1-D PCL) embedded in a high-index cubical prism is presented. The PBS is based on index matching and total transmission for the p polarization and total internal reflection for the s polarization at the prism-PCL interface at a 45^o angle of incidence. A high extinction ratio in reflection (>50 dB) over the 4-12 μm IR spectral range is achieved using a SWS 1-D PCL of ZnTe embedded in a ZnS cube within an external field of view (FOV) of $\pm 6.6^o$ and in the presence of grating filling factor errors of up to $\pm 10\%$. Comparable results, but with a wider field of view, are also obtained with a Ge PCL embedded in a Si prism. A design for visible spectrum (553–713 nm) PBS SWS 1-D PCL of ZnTe embedded in a ZnS cube is also presented. The PBS shows a FOV of $\pm 7^o$.

A circular polarizing beam splitter (CPBS) with equal throughput for p and s polarization using SWS 1-D PCL embedded in a high-index cubical prism is introduced. A dual QWR in transmission and reflection with 50–50% CPBS is designed using the PCL. Such a

CPBS shows large deviation from the design point as a result of small changes in the design parameters; e.g. a change of $\approx 10\%$ in the filling factor results in $> 12^o$ shift from the 90^o phase shift between p and s polarizations, which limits the practical utility of the device.

Keywords: Beam Splitters, Form Birefringence, Gratings, Photonic Crystal, Polarization, Quarter-Wave Retarder.

Chapter 1

Introduction

1.1 Motivation

High extinction ratio and wide field of view (FOV) are important features of polarizing beam splitters (PBS). Use of photonic-crystal layers embedded in high-refractive-index cubic prism enable PBS with high extinction ratio and wide FOV over an extended range of wavelengths. This is demonstrated in detail in Chapters 3–6.

1.2 Quarter-Wave Retarders

Quarter-wave retarders are widely used for changing the state of polarization of incident light by introducing a 90^o phase shift between the two orthogonal p and s linear polarizations [1]-[2]. QWR can be achieved by transmission through wave-plates [3] or by using QWR prisms of different designs that employ one or multiple total internal reflection (TIR) reflection [4]-[10].

To achieve QWR on a single TIR at a dielectric-dielectric interface requires a refractive index ratio $\geq \sqrt{2}+1 = 2.414$ [11]. A non-interference-coating may be used to attain QWR on a single TIR [12]. However, an interference-coating significantly alters the phase shifts that accompany TIR, hence introducing flexibility that can be exploited in the design of QWR [13],[14].

In Chapter 2 we introduce a new analytical approach for the design of TIR QWR using a single-layer interference coating and provide several examples of its application.

1.3 Photonic Crystals

Photonic crystals are periodic structures that consist of different refractive index materials. The variation of the refractive index can be along one, two, or three axes, as shown in Fig. 1.1 [20]. Photonic crystals are presentd as one dimensional (1-D) [21]-[23], two dimensional (2-D) [24]-[29], or three dimensional (3-D) [30]-[32].

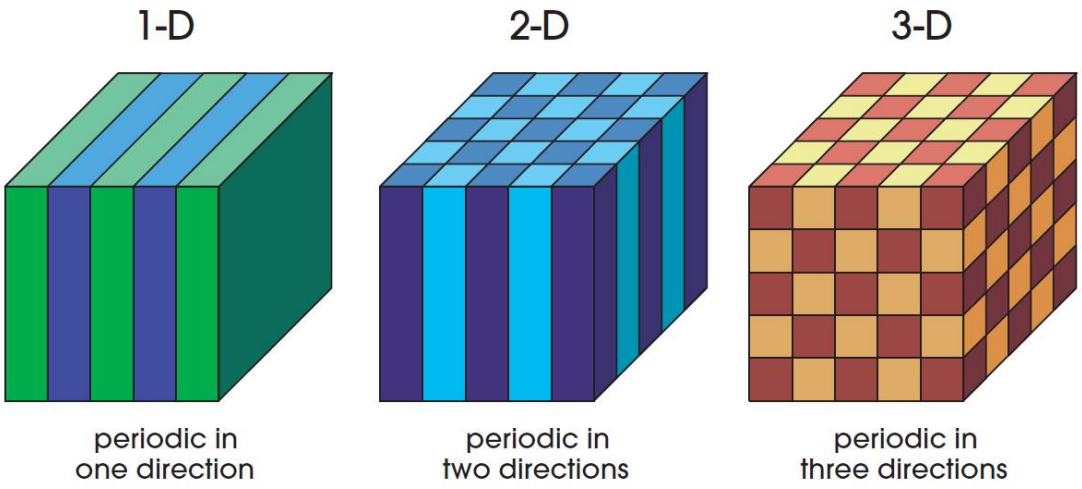

Figure 1.1: Simple examples of one-, two-, and three-dimensional photonic crystals. Different colors represent different refractive indices.

The use of photonic crystals is spread out in many applications that include polarizing beam splitters [33]-[37], polarizers [40]-[41], polarization rotators [42]-[43], wave retarders [44]-[46], photonic-crystal fibers [48]-[49], and anti-reflection coatings [50]-[53].

1.4 Polarizing Beam Splitters

PBSs are used to separate the orthogonal p and s linear polarization components of an incident light beam into two beams that travel in different directions. Conventional PBSs employ crystal optics [1] or multilayer interference coatings that are embedded in a prism

[54]-[58]. More recently, PBSs that use diffraction gratings [59]-[63] and photonic crystals [33]-[37] have also been introduced.

In Chapters 3–6 PBSs are introduced that use the form birefringence of subwavelength-structured (SWS) layers embedded in a high-index prism. The non-diffracting SWS 1-D photonic–crystal layer (PCL) is equivalent to a homogeneous uniaxial crystal with the optic axis normal to the plane of incidence. The p polarization is totally transmitted and the s polarization is totally internally reflected.

1.5 Applications of Polarizing Beam Splitters

PBSs are used in the division–of–amplitude polarimeter [38] as shown in Fig. 1.2 to measure the stokes parameters of light which describe its state of polarization.

Also, PBSs are used in optical storage systems. The PBS divide the incident light into two beams to reduce the optical noise. One beam is used to monitor the light intensity and the other is used to read and write the data on the disk [39].

1.6 Circular Polarizing Beam Splitter

A circular polarizing beam splitter (CPBS) is used to separate an incoming linearly polarized beam into two circularly polarized beams that travel in different directions. CPBSs that em-

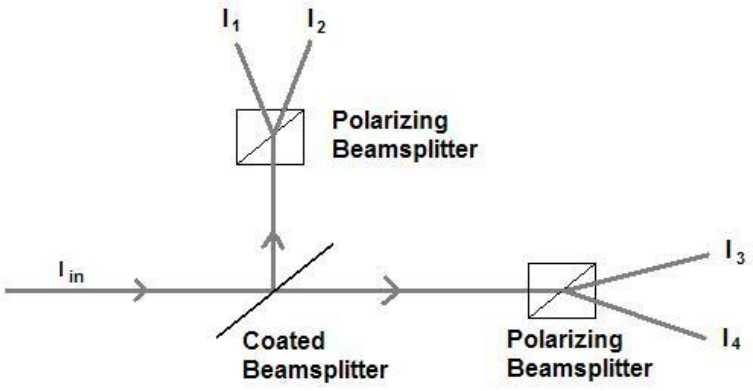

Figure 1.2: A setup of a division–of–amplitude polarimeter

ploy liquid-crystal gratings [64], symmetrically coated pellicles [65], frustrated total internal reflection by an embedded symmetric trilayer [66], optical tunneling through an embedded film [67], or photonic crystal [68] have also been introduced.

In Chapter 7 a 50-50% BS with dual quarter-wave retarder in reflection and transmission is introduced that uses the form birefringence of a SWS embedded PCL in a high-index prism. The non-diffracting SWS 1-D PCL is equivalent to a homogeneous uniaxial crystal with the optic axis normal to the plane of incidence. Finally, Chapter 8 gives a brief summary of the work.

Chapter 2

Quarter-Wave Retarders Based on Total Internal Reflection and Light Interference in Single-Layer Coating

2.1 Introduction

Quarter-wave retarders are used to alter the state of polarization of incident light from linear to circular or vice versa by introducing a 90^o phase shift between the two orthogonal p and s linear polarizations.

2.2 Design Procedure

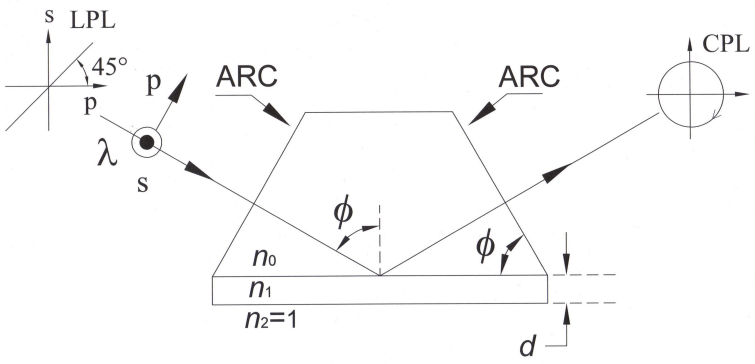

Figure 2.1: TIR of a monochromatic light beam of wavelength λ at an angle of incidence ϕ at the base of a prism of refractive index n_0 which is coated with a transparent thin film of refractive index n_1 and thickness d. The entrance and exit faces of the prism are anti-reflection coated (ARC). p and s represent the orthogonal linear polarizations parallel and perpendicular to the plane of incidence, respectively.

Figure 2.1 shows the TIR of monochromatic light with wavelength λ at angle of incidence ϕ at the base of a prism with refractive index n_0 coated by a thick film layer with refractive index n_1 and thickness d. The outside ambient surrounding is assumed to be air ($n_2 = 1$) and the entrance and exit faces are assumed to have anti-reflection coating (ARC) and normal to incident light. The complex amplitudes of the linear parallel polarization p and perpendicular s polarization to the plain of of incidence [2] are given by

$$R_\nu = \frac{r_{01\nu} + r_{12\nu} X}{1 + r_{01\nu} r_{12\nu} X}, \nu = p, s. \tag{2.1}$$

where $r_{01\nu}$ and $r_{12\nu}$ are Fresnel reflection coefficients at the prism-film and film-ambient interfaces for the ν polarization, respectively, and

$$\begin{aligned} X &= \exp(-i2\pi\varsigma) \\ \varsigma &= \frac{d}{D_\phi} \\ D_\phi &= \frac{\lambda}{2}(n_1^2 - n_0^2 \sin^2\phi)^{-\frac{1}{2}} \end{aligned} \tag{2.2}$$

TIR at the film-ambient interface requires that the angle of incidence $\phi_{02} > \phi_{c02} = \arcsin(\frac{1}{n_0})$, where ϕ_{c02} is the critical angle of the prism–ambient (02) interface. Also, $n_1 > n_0$ is required to ensure partial reflection at the prism-film (01) interface so that light interference is allowed in the coating film. Under these conditions, R_ν in Eq. (2.1) are periodic functions of film thickness d with period D_ϕ given in Eq. (2.2).

The reflection coefficients $r_{01\nu}$ and $r_{12\nu}$ of Eq. (2.1) can be expressed as functions of two angles α_ν and δ_ν,

$$\begin{aligned} r_{01\nu} &= \tan\alpha_\nu, \\ r_{12\nu} &= \exp(i\delta_\nu), \\ \nu &= p, s. \end{aligned} \tag{2.3}$$

In the Nebraska-Muller conventions [2],[15] α_ν and δ_ν are restricted to the following ranges,

$$\begin{aligned} -45^o &\leq \alpha_p \leq 45^o, \\ -45^o &\leq \alpha_s \leq 0, \\ 0 &\leq \delta_{p,s} \leq \pi. \end{aligned} \tag{2.4}$$

By substituting Eqs. (2.2) and (2.3) into Eq. (2.1), we obtain

$$\begin{aligned} R_\nu &= \frac{\tan\alpha_\nu + \exp(-i\gamma_\nu)}{1 + \tan\alpha_\nu \exp(-i\gamma_\nu)}, \\ \gamma_\nu &= 2\pi\varsigma - \delta_\nu, \\ \nu &= p, s. \end{aligned} \tag{2.5}$$

From Eq. (2.5), $R_\nu R_\nu^* = -1$, which confirms that TIR occurs at the coated base of the prism. Consequently, R_ν can be expressed as a pure phase factor,

$$R_\nu = \exp(i\Delta_\nu), \nu = p, s. \tag{2.6}$$

In Eq. (2.6), Δ_ν is the overall TIR phase shift for the ν polarization. From Eqs. (2.5) and (2.6) we obtain

$$\tan\Delta_\nu = \frac{-\cos(2\alpha_\nu)\sin\gamma_\nu}{\sin(2\alpha_\nu) + \cos\gamma_\nu}, \nu = p, s. \tag{2.7}$$

The differential retardance on TIR is given by

$$\Delta = \Delta_p - \Delta_s \tag{2.8}$$

Taking the tangent of both sides of Eq. (2.8)

$$\tan\Delta = \frac{\tan\Delta_p - \tan\Delta_s}{1 + \tan\Delta_p \tan\Delta_s} \tag{2.9}$$

To achieve QWR (differential retardance of $\Delta = \pm\frac{\pi}{2}$) on TIR, the denominator of Eq.(2.9) should equal to zero, so that

$$\tan\Delta_p \tan\Delta_s = -1 \tag{2.10}$$

Substituting Eq. (2.7) in Eq. (2.10)

$$\begin{aligned}&\cos\gamma_p\cos\gamma_s + \sin(2\alpha_p)\cos\gamma_s + \sin(2\alpha_s)\cos\gamma_p + \cos(2\alpha_p)\cos(2\alpha_s)\sin\gamma_p\sin\gamma_s \\ &+ \sin(2\alpha_p)\sin(2\alpha_s) = 0,\end{aligned} \tag{2.11}$$

where α_p, α_s, δ_p, and δ_s are given by

$$\begin{aligned}\alpha_p &= \frac{\pi}{4} - \arctan\left\{\frac{n_0(n_1^2 - n_0^2\sin^2\phi)^{\frac{1}{2}}}{n_1^2\cos\phi}\right\}, \\ \alpha_s &= \frac{\pi}{4} - \arctan\left\{\frac{(n_1^2 - n_0^2\sin^2\phi)^{\frac{1}{2}}}{n_0\cos\phi}\right\},\end{aligned} \tag{2.12}$$

$$\begin{aligned}\gamma_p &= 2\pi\varsigma - 2\arctan\left\{\frac{n_1^2(n_0^2\sin^2\phi - 1)^{\frac{1}{2}}}{(n_1^2 - n_0^2\sin^2\phi)^{\frac{1}{2}}}\right\}, \\ \gamma_s &= 2\pi\varsigma - 2\arctan\left\{\frac{(n_0^2\sin^2\phi - 1)^{\frac{1}{2}}}{(n_1^2 - n_0^2\sin^2\phi)^{\frac{1}{2}}}\right\}.\end{aligned} \tag{2.13}$$

Equation (2.11) represents the essential design condition for achieving QWR using TIR by a single-layer-coated prism (Fig. 2.1). For given prism refractive index n_0 and angle of incidence ϕ, Eq. (2.11) can be written as

$$f(n_1, \varsigma) = 0 \tag{2.14}$$

where f is a function of the refractive index n_1 and normalized thickness ς of the interference coating. As will be shown, there are infinitely many solutions for Eq. (2.11), but there is only one optimal solution with minimum sensitivity to small changes of the normalized film

thickness ς or wavelength λ.

2.3 Total Internal Reflection QWR Using Coated Glass Prism

A glass prism of refractive index $n_0 = 1.5$ and an angle of incidence $\phi = 60^o$ are assumed in our design of the QWR on TIR.

Figure 2.2 shows a plot of $f(n_1,\varsigma)$ as the normalized thickness is varied $0 \leq \varsigma \leq 1$ for constant values of n_1 from 1.9 to 5.9 with uniform steps of 0.2. For each n_1 curve in this range, Eq. (2.11) has two solutions for ς [for $n_1 = 1.9$, points **A** and **B** are the two solutions of Eq. (2.14)]. The minimum value of n_1 for which the two solutions overlap is $n_{1min} = 1.7924$ and the corresponding value of $\varsigma = 0.335$ is represented by point **C**. This point of tangency with the curve $f(n_1,\varsigma)$=0 represents the optimal choice of the film refractive index and thickness as it indicates insensitivity to small changes of ς, hence tolerance to small film-thickness errors or wavelength shifts. Suitable optical coating materials whose refractive index can be tuned to the optimal value $n_{1min} = 1.7924$ (e.g. by appropriate control of stoichiometry and deposition conditions) include SiON [16] and Y_2O_3 [17].

Figure 2.3 shows the locus of all possible solutions of Eq. (2.14) for QWR coatings on glass of refractive index $n_0 = 1.5$ at an angle of incidence $\phi = 60^o$. The optimal film coating refractive index and thickness correspond to point **C** at the bottom of the curve.

Figure 2.4 shows optimal (minimum) refractive index n_{1min} and associated normalized thickness ς of thin-film coatings on a glass prism ($n_0 = 1.5$) that achieve QWR on TIR at angles of incidence ϕ that vary from 45^o to 75^o.

Figure 2.5 shows optimal (minimum) refractive index n_{1min} and associated normalized thickness ς of thin-film coatings on ZnS [18] prism ($n_0 = 2.35$) that achieve QWR on TIR at angles of incidence ϕ that vary from 45^o to 75^o.

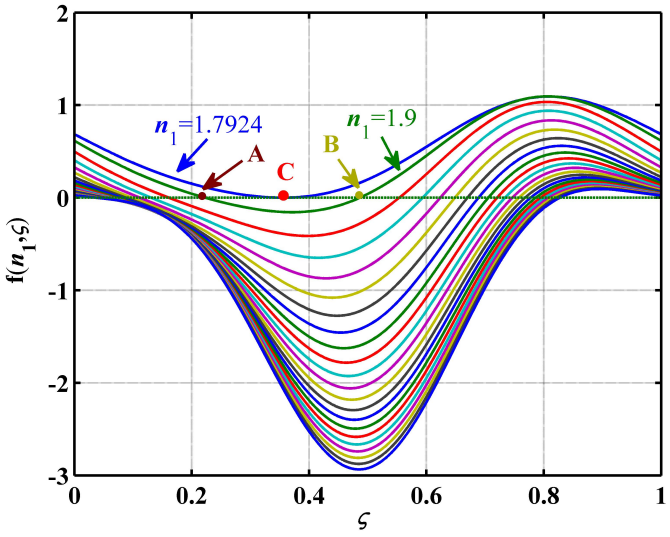

Figure 2.2: A plot of $f(n_1,\varsigma)$ as a function of ς for constant value of n_1 from 1.9 to 5.9 in a uniform step of 0.2. For each n_1 curve, Eq. (2.14) has two solutions for ς (for $n_1 = 1.9$, points **A** and **B** are the two solutions of Eq. (2.14)). The minimum value of n_1, for which the two solutions overlap is $n_{1min} = 1.7924$ at point **C**.

2.4 Spectral Response of TIR QWR that Uses Right-Angle Prism of N-BK10 Glass Coated with Si_3N_4 Film

In this section we consider a design of QWR on TIR using a right-angle prism ($\phi = 45^o$) of N-BK10 schott glass with refractive of index $n_0 = 1.5021$ [19] at wavelength $\lambda = 500$ nm. The calculated optimal value of the refractive index of the coating film $n_1 = 2.0607$ matches that of silicon nitride (Si_3N_4) [17] at wavelength $\lambda = 500$ nm, with the associated optimal film thickness $d = 43.66$ nm.

Figure 2.6 shows the spectral response Δ as a function of λ, for $400 \leq \lambda \leq 600$ nm of TIR QWR where the dispersion of coating film and prism refractive indices [16],[19] are taken into account. QWR on TIR is achieved at the design wavelength $\lambda = 500$ nm and also at the shorter wavelength $\lambda = 409$ nm, as represented by points **P** and **Q**, respectively. The deviation of Δ from exact QWR ($\Delta = 90^o$) is $< 0.5^o$ for 400 nm$\leq \lambda \leq 520$ nm and $\approx 3^o$ at $\lambda = 600$ nm. Therefore, good achromatic performance is attained over a substantial portion of the visible spectrum.

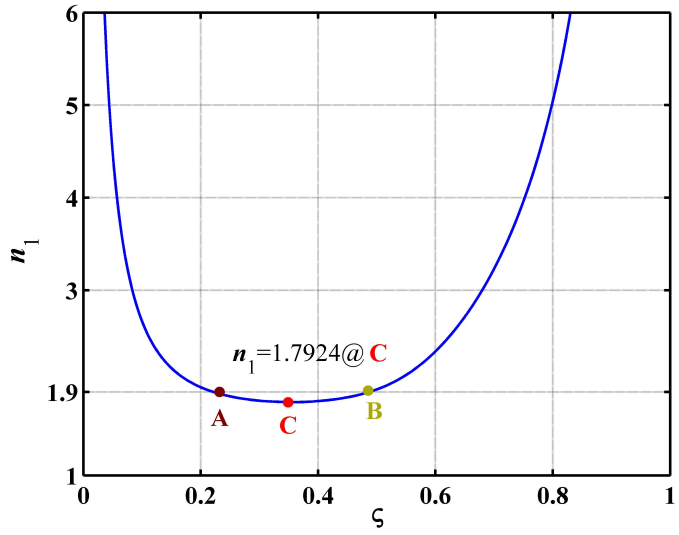

Figure 2.3: Locus of all possible solutions of Eq. (2.14) is shown for coatings on glass of refractive index $n_0 = 1.5$ that achieve QWR on TIR at an angle of incidence $\phi = 60^o$. The optimal coating is represented by point **C**.

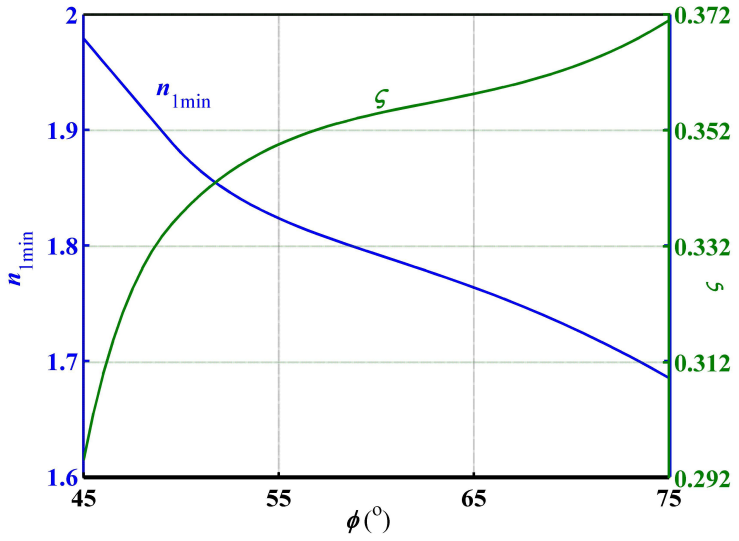

Figure 2.4: Optimal (minimum) refractive index n_{1min} and associated normalized thickness ς of thin-film coatings on glass prism ($n_0 = 1.5$) that achieve QWR on TIR at angles of incidence ϕ that vary from 45^o to 75^o.

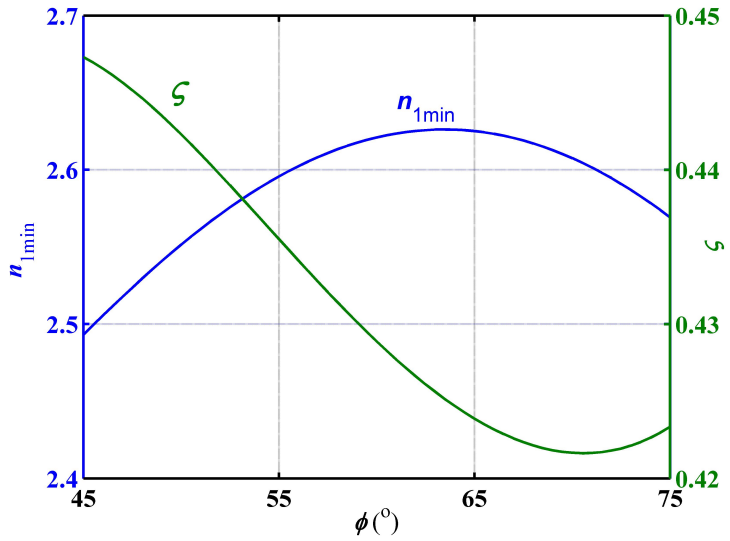

Figure 2.5: Optimal (minimum) refractive index n_{1min} and associated normalized thickness ς of thin-film coatings on ZnS prism ($n_0 = 2.35$) that achieve QWR on TIR at angles of incidence ϕ that vary from 45^o to 75^o.

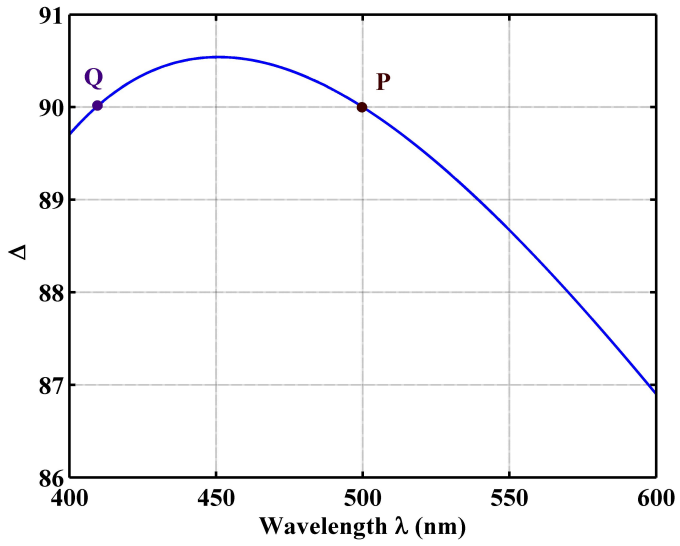

Figure 2.6: Spectral response Δ versus λ of TIR QWR for a right-angle prism ($\phi = 45^o$) of N-BK10 Schott glass with refractive index $n_0 = 1.5021$ at $\lambda = 500$ nm. The base of the prism is coated with a silicon nitride layer of refractive index $n_1 = 2.0607$ ($\lambda = 500$ nm) and metric thickness $d = 43.66$ nm. QWR is exactly achieved at wavelengths of $\lambda = 500$ and $\lambda = 409$ nm (points **P** and **Q**, respectively).

Chapter 3

Polarizing Beam Splitters Using Subwavelength-Structured 1-D PCL Embedded in High-Index Prism

3.1 Introduction

A polarizing beam splitter (PBS) separates the orthogonal p and s linear polarization components of an incident light beam into two beams that travel in different directions.

3.2 Design Procedure

The 1-D PCL is shown in Fig. 3.1 with its optic axis parallel to the grating vector. Figure 3.1(a) shows the cross section of a 1-D PCL of thickness d that consists of rectangular grating of a coating material of refractive index n_c, grating period Λ, and filling factor f. The layer is deposited on an optically isotropic substrate (prism) of refractive index n. Figure 3.1(b) shows the PBS cube with the grating vector $\overrightarrow{K}_G$ of the PCL normal to the plane of incidence. p and s denote the linear polarizations parallel and perpendicular to the plane of incidence, respectively.

With $\lambda \gg \Lambda$ the 1-D PCL equivalent to a non-diffracting homogeneous uniaxial crystal layer with its optic axis parallel to the grating vector. The effective, second-order, ordinary (o) and extraordinary (e) refractive indices of the 1-D PCL with its optic axis parallel to the

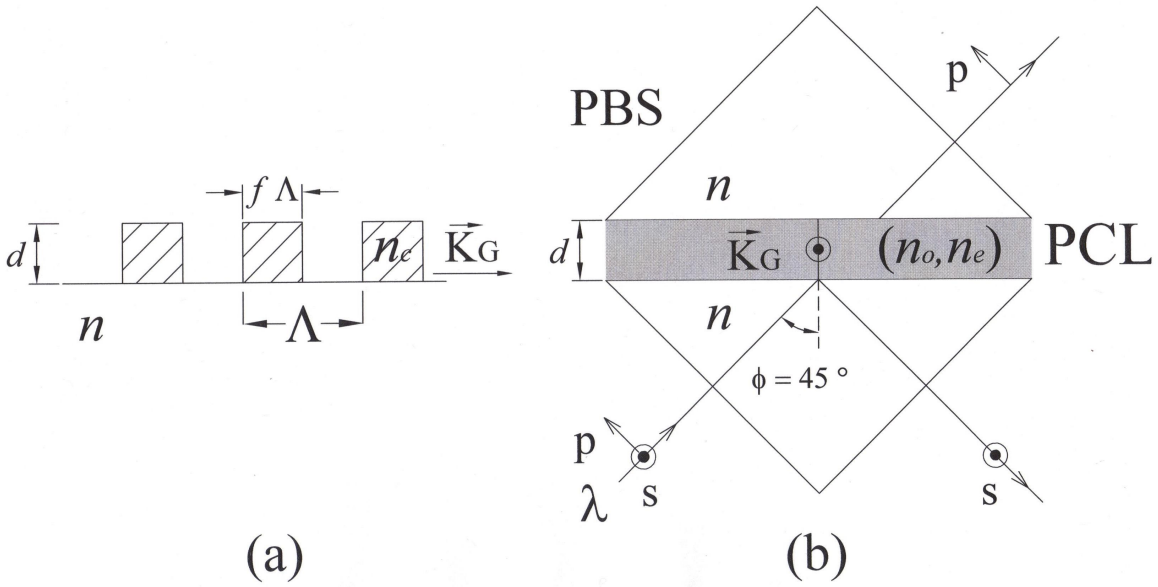

Figure 3.1: (a) Cross section of a 1-D PCL of thickness d that consists of a rectangular grating of a coating material of refractive index n_c, grating period Λ, and filling factor f. The layer is deposited on an optically isotropic substrate (prism) of refractive index n. (b) PBS cube with the grating vector $\vec{K}_G$ of the PCL normal to the plane of incidence. p and s denote the linear polarizations parallel and perpendicular to the plane of incidence, respectively.

grating vector are determined by [69],

$$n_o^{(2)} = \left\{ (n_o^{(1)})^2 + \frac{1}{3}\left[\pi\frac{\Lambda}{\lambda} f(1-f)\right]^2 (n_c^2 - 1)^2 \right\}^{\frac{1}{2}} \tag{3.1}$$

$$n_e^{(2)} = \left\{ (n_e^{(1)})^2 + \frac{1}{3}\left[\pi\frac{\Lambda}{\lambda} f(1-f)\right]^2 (\frac{1}{n_c^2} - 1)^2 (n_e^{(1)})^6 (n_o^{(1)})^2 \right\}^{\frac{1}{2}} \tag{3.2}$$

where

$$\begin{aligned} n_o^{(1)} &= (1 - f + n_c^2 f)^{\frac{1}{2}} \\ n_e^{(1)} &= (1 - f + f\frac{1}{n_c^2})^{-\frac{1}{2}} \end{aligned} \tag{3.3}$$

are the first–order indices that are independent of Λ/λ.

As shown in Fig. 3.1(b), the grating vector is normal to the plane of incidence and the p polarization sees the ordinary index of PCL $n_o = n_o^{(2)}$ [the superscript $^{(2)}$ is dropped for

simplicity], and experiences zero reflection if

$$n_o = n, \tag{3.4}$$

independent of the angle of incidence. The index-matching condition (between the substrate index and the 1-D PCL ordinary index) of Eq.(3.4) allows the p polarization to be totally transmitted. One the other hand, the s polarization sees the extraordinary refractive index of PCL $n_e = n_e^{(2)}$ and experiences total internal reflection at the isotropic prism–PCL interface if the critical angle $\phi_{cs} < 45^o$, so that

$$\begin{aligned} \phi_{cs} &= \sin^{-1} x \\ x &= \frac{n_e}{n} < \frac{1}{\sqrt{2}} \end{aligned} \tag{3.5}$$

To avoid partial optical tunneling of the s polarization, the thickness d of the PCL must be $>>$ the penetration depth of the s component wave. This condition is assumed to hold and interference effects in the PCL are ignored in this section. From Eqs. (3.4) and (3.5) we obtain

$$n_e = x n_o \tag{3.6}$$

Finally, substitution of n_o and n_e from Eqs. (3.1) and (3.3) in Eq. (3.6) yields one key equation in the three design parameters x, n_c, and f :

$$\begin{aligned} &(1 - f + f\frac{1}{n_c^2})^{-1} + \frac{1}{3}[\pi\frac{\Lambda}{\lambda}f(1-f)]^2(\frac{1}{n_c^2} - 1)^2(1 - f + f\frac{1}{n_c^2})^{-3}(1 - f + n_c^2 f) = \\ &x^2\big\{(1 - f + n_c^2 f) + \frac{1}{3}[\pi\frac{\Lambda}{\lambda}f(1-f)]^2(n_c^2 - 1)^2\big\} \end{aligned} \tag{3.7}$$

The iterative steps used for designing a PBS are shown in the flowchart of Fig. 3.2 for a given wavelength λ and grating period Λ.

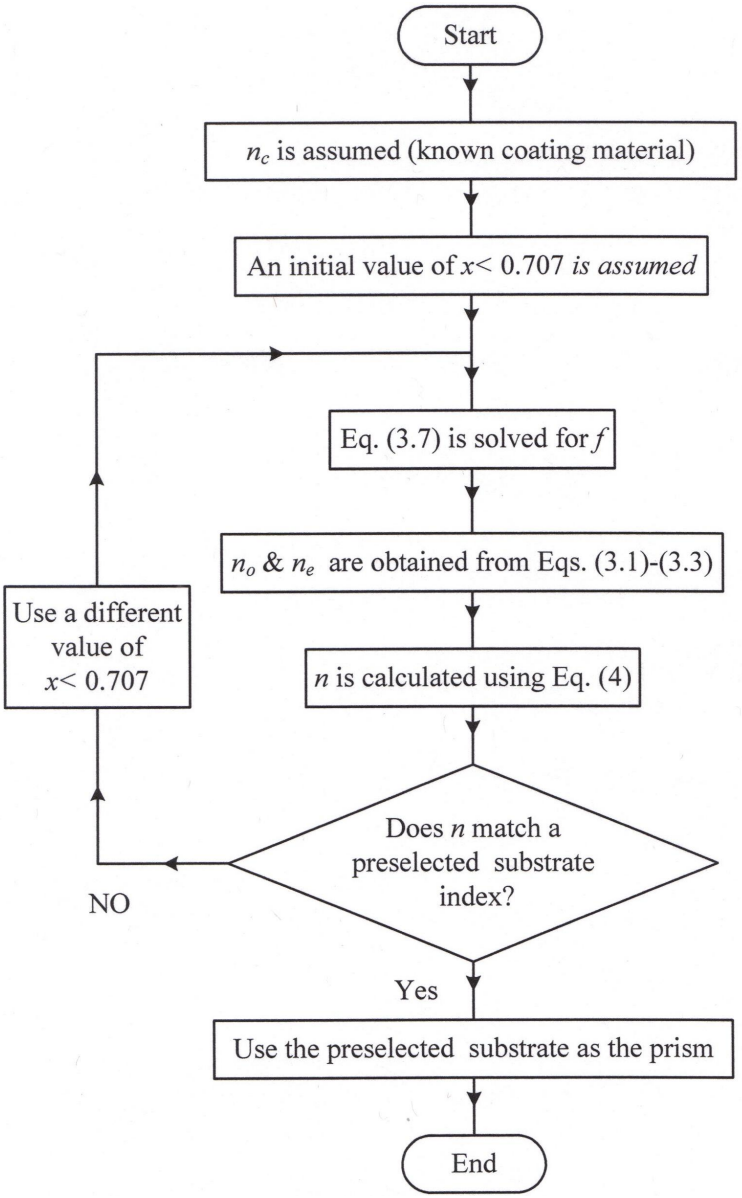

Figure 3.2: Iterative design steps for a PBS that operates at a given wavelength λ and grating period $\Lambda \gg \lambda$.

Chapter 4

Broadband IR PBS Using ZnTe Photonic-Crystal Layer Embedded in ZnS Cube

4.1 Introduction

PBS design that uses a ZnTe 1-D PCL (grating), which is embedded between two right-angle ZnS prisms, is presented for the CO_2- laser wavelength 10.6 μm, with grating period $\Lambda = 1$ μm and n_c(ZnTe) = 2.6818 [70]. By applying the iterative steps shown in Fig. 3.2 with $x = 0.6669$, we obtain $\phi_{cs} = 41.8314^o$, $f = 0.6042$, $n_o = 2.1921$, and $n_e = 1.4620$. This represents a PCL with giant negative birefringence $\Delta n = n_e - n_o = -0.71$. For index matching of n_o and n, ZnS is chosen as a prism which has refractive index $n = 2.1921$ at λ =10.6 μm [70]. Design parameters for a PBS using ZnTe PCL embedded in a ZnS cube at wavelength 10.6 μm are listed in Table 4.1.

4.2 Non-Interference Photonic-Crystal Layer of ZnTe Embedded in ZnS Cube

Table 4.1: Design parameters for PBS using ZnTe PCL with grating period $\Lambda = 1\mu$m embedded in ZnS cube at wavelength $\lambda = 10.6$ μm

n_c(ZnTe)	f	n_e	n_o	n(ZnS)	ϕ_{cs}
2.6818	0.6042	1.4620	2.1921	2.1921	41.8314^o

The Fresnel reflection coefficients for the incident linear polarizations parallel p and

perpendicular s to the plane of incidence at the prism–PCL interface are given by [2]:

$$r_{01p} = \frac{n_o^2 \cos\phi_0 - n(n_o^2 - n^2 \sin^2\phi_0)^{\frac{1}{2}}}{n_o^2 \cos\phi_0 + n(n_o^2 - n^2 \sin^2\phi_0)^{\frac{1}{2}}} \tag{4.1}$$

$$r_{01s} = \frac{n \cos\phi_0 - (n_e^2 - n^2 \sin^2\phi_0^2)^{\frac{1}{2}}}{n \cos\phi_0 + (n_e^2 - n^2 \sin^2\phi_0)^{\frac{1}{2}}} \tag{4.2}$$

An important performance parameter of the PBS is its reflection extinction ratio

$$ER_r = 10 \log_{10} \frac{R_s}{R_p} \tag{4.3}$$

The reflection of the p polarization is independent of the angle of incident ϕ due to index matching ($n_o = n$) while the reflection coefficient r_s of the s polarization depends on ϕ. Figure 4.1 shows the intensity reflectance R_s of s polarization as a function of the angle of incidence ϕ at the prism(ZnS)-PCL(ZnTe) interface using Eq. (4.2), with grating period $\Lambda = 1$ μm and filling factor $f = 0.6042$ at wavelength $\lambda = 10.6$ μm. As shown in Fig. 4.1 the critical angle $\phi_{cs} = 41.8314^o$ is 3^o away from the design angle of incidence $\phi = 45^o$ which gives an internal field of view (FOV) of $\pm 3^o$. A corresponding external (in-air) FOV of $\pm n \times 3^o = 6.6^o$ is obtained by applying Snell's law.

Figure 4.2 shows the intensity reflectance R_p of p polarization versus the filling factor f as it is changed by $\approx \pm 10\%$ around the design value $f = 0.6042$, with all other parameters kept constant. Changing the filling factor affects the effective refractive indices of the PCL n_o and n_e as indicated by Eqs. (3.1) and (3.2), respectively. This variation leads to mismatch between the ordinary refractive index of the PCL and the prism refractive index $n_o \neq n$. As a result, the reflection coefficient r_p of the p polarization deviate from zero and a portion of the p polarization is reflected. However, this reflection is very small, $R_p < 1.4\text{x}10^{-6}$. On the other hand, the s polarization is not affected by this change of filling factor $0.455 \leq f \leq 0.654$ and is totally reflected ($R_s = 1$).

Figure 4.3 shows the extinction ratio in reflection ER_r vs the filling factor f as it is

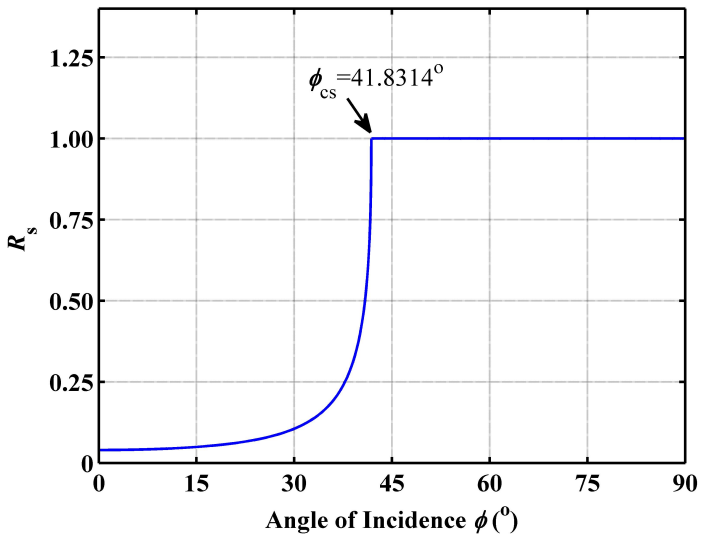

Figure 4.1: Intensity reflectance R_s of s polarization as a function of the angle of incidence ϕ at the prism(ZnS)-PCL(ZnTe) interface, with grating period $\Lambda = 1$ μm and filling factor $f = 0.6042$ at wavelength $\lambda = 10.6$ μm.

changed by $\approx \pm 10\%$ around the design value $f = 0.6042$, with all other parameters kept constant. The maximum value of the extinction ratio $ER_r \approx 273$ dB which diminished to $ER_r \approx 59$dB as the filling factor ranged from 0.455 to 0.654, which indicates good tolerance to small dimensional errors.

Figure 4.4 shows the deviation from index matching of p polarized light (i.e., $n_o = n$) as the wavelength is varied $4 \leq \lambda \leq 12$ μm for the prism of ZnS and and PCL of ZnTe, with all other parameters kept constant. As shown in Fig. 4.4, the refractive index matching ($n_o = n$) occurs at the design wavelength $\lambda = 10.6$ μm and unexpectedly, also at $\lambda = 5.5$ μm. The dispersion of the coating and prism materials is considered [70] and the unity intensity reflectance of s polarization ($R_s = 1$) is maintained over the entire bandwidth $4 \leq \lambda \leq 12$ μm.

Figure 4.5 shows the intensity reflectance R_p of p polarization as a function of wavelength λ, for $4 \leq \lambda \leq 12$ μm, with all other parameters kept constant. The minimum reflection of p polarization (maximum transmission) $R_p \approx 0$ takes place at the design wavelength $\lambda = 10.6$ μm and also at $\lambda = 5.5$ μm which is consistent with Fig. 4.4. The maximum intensity

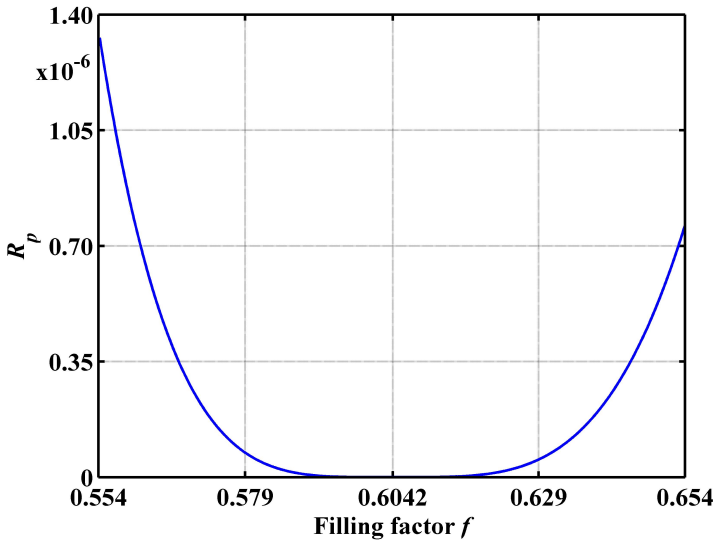

Figure 4.2: Intensity reflectance R_p of p polarization as a function of the filling factor f at the prism(ZnS)-PCL(ZnTe) interface, with angle of incidence $\phi = 45^o$ and grating period $\Lambda = 1$ μm at wavelength $\lambda = 10.6$ μm.

reflectance R_p is 1.4×10^{-6} for the entire bandwidth $4 \leq \lambda \leq 12$ μm.

Figure 4.6 shows the extinction ratio in reflection ER_r as a function of wavelength λ, for $4 \leq \lambda \leq 12$ μm, with all other parameters kept constant. Notice that the ER_r is > 70 dB over the full spectral range and spikes at the design wavelength $\lambda = 10.6$ μm and also at $\lambda = 5.5$ μm, consistent with Figs. 4.4 and 4.5. Therefore, near-ideal broadband PBS is achieved.

4.3 Interference Effects within the Photonic-Crystal Layer of ZnTe Embedded in ZnS Cube

In Section 4.2 the effects of interference were ignored and the thickness of the layer d was assumed to be $\gg$ penetration depth of the s polarization component wave into the PCL. For a practical design the layer thickness should be defined. In this section PCL with two different thicknesses d=10 μm and d=20 μm is considered, and the performance of the PBS is calculated and compared for both thicknesses.

The complex–amplitude reflection coefficients for the p and s polarizations are given by [2]:

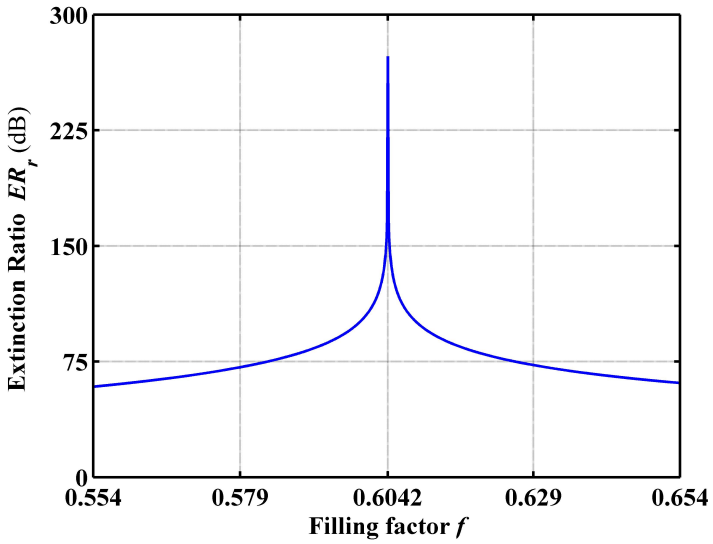

Figure 4.3: Extinction ratio in reflection ER_r vs the filling factor f at the prism(ZnS)-PCL(ZnTe) interface, for angle of incidence $\phi = 45^o$, grating period $\Lambda = 1$ μm, and wavelength $\lambda = 10.6$ μm.

$$r_p = \frac{r_{01p} - r_{01p}e^{-j2\beta_p}}{1 - r_{01p}^2 e^{-j2\beta_p}} \tag{4.4}$$

$$r_s = \frac{r_{01s} - r_{01s}e^{-j2\beta_s}}{1 - r_{01s}^2 e^{-j2\beta_s}} \tag{4.5}$$

where β_p and β_s are given by:

$$\beta_p = 2\pi(\frac{d}{\lambda})(n_o^2 - n^2 \sin^2 \phi_0)^2 \tag{4.6}$$

$$\beta_s = 2\pi(\frac{d}{\lambda})(n_e^2 - n^2 \sin^2 \phi_0)^2 \tag{4.7}$$

and r_{01p} and r_{01s} are given by Eqs. (4.1) and (4.2), respectively.

Figure 4.7 shows the intensity reflectance R_p of p polarization at the prism(ZnS)-PCL(ZnTe) interface as a function of the filling factor f for $d = 10$ μm and $d = 20$ μm, with all other parameters kept constant. $R_p \approx 0$ for both designs at the design filling factor $f = 0.6042$. However, the design with $d = 10$ μm shows a smaller reflection as f is away from the design point, which is consistent with Fig. 4.2.

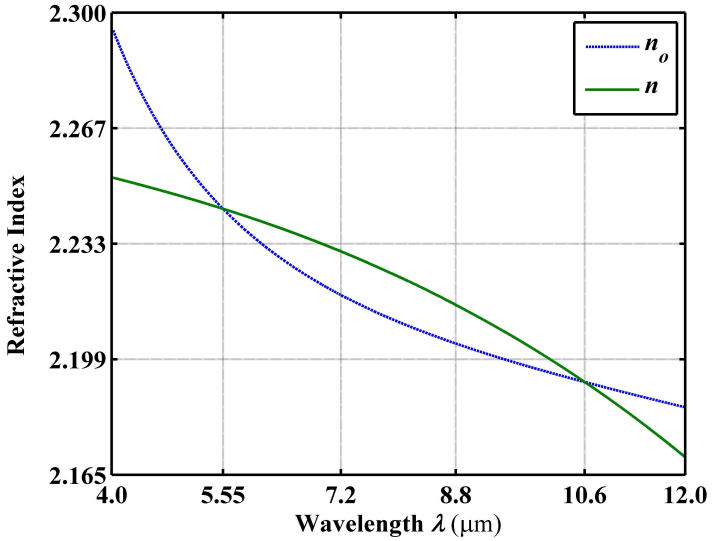

Figure 4.4: Deviation from index matching of p polarized light as the wavelength λ is varied $4 \leq \lambda \leq 12$ μm for the prism of ZnS and and PCL of ZnTe, with angle of incidence $\phi = 45^o$, grating period $\Lambda = 1\mu$m, taking into account dispersion of the optical properties of ZnTe and ZnS.

Figure 4.8 shows the extinction ratio in reflection ER_r as a function of the filling factor f for layer thicknesses $d = 10$ μm and $d = 20$ μm, with all other parameters kept constant. As expected, a spike appears at the design point $f = 0.6042$, and another spike appears at $f = 0.6249$.

Figure 4.9 shows the intensity reflectance R_p of p polarization at the prism(ZnS)-PCL(ZnTe) interface as a function of the wavelength λ, for $4 \leq \lambda \leq 12$ μm for layer thicknesses $d = 10$ μm and $d = 20$ μm, with all other parameters kept constant. The interference oscillations of $R_p < 2 \times 10^{-6}$. Excellent performance is maintained when interference effects in the PCL are taken into consideration.

Figure 4.10 shows intensity reflectance R_s of s polarization at the prism(ZnS)-PCL(ZnTe) interface as a function of of the wavelength λ for layer thicknesses $d = 10$ μm and $d = 20$ μm, with all other parameters kept constant. R_s falls off monotonically as λ increases and d decreases, which is consistent with the expected increase in optical tunneling as $\frac{d}{\lambda}$ decreases.

Figure 4.11 shows extinction ratio in reflection ER_r as a function of wavelength Λ, for $4 \leq \lambda \leq 12$ μm for layer thicknesses $d = 10$ μm and $d = 20$ μm, with all other parameters

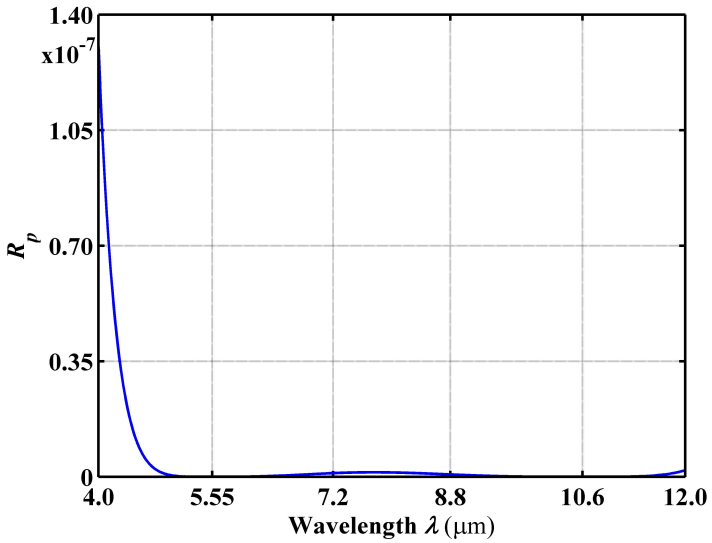

Figure 4.5: Intensity reflectance R_p of p polarization as a function of the wavelength λ at the prism(ZnS)-PCL(ZnTe) interface, with angle of incidence $\phi = 45^o$ and grating period $\Lambda = 1$ μm at filling factor $f = 0.6042$.

kept constant. Multiple spikes appear which correspond to and are consistent with $R_p = 0$ of Fig. 4.9. ER_r is > 70 dB for the entire bandwidth $4 \leq \lambda \leq 12$ μm which indicates near ideal polarization on reflection.

Figure 4.12 shows the extinction ratio in transmission ER_t

$$ER_t = 10 \log_{10} \frac{T_p}{T_s} = 10 \log_{10} \frac{1 - R_p}{1 - R_s} \tag{4.8}$$

as a function of the wavelength λ, for $4 \leq \lambda \leq 12$ μm for layer thicknesses $d = 10$ μm and $d = 20$ μm, with all other parameters kept constant. The design with $d = 20$ μm shows a higher extinction ratio. This is consistent with the decrease of R_s as $\frac{d}{\lambda}$ decreases, caused by increased optical tunneling.

Figure 4.13 shows the extinction ratio in transmission as a function of the layer thickness d, with all other parameters kept constant. Higher values of ER_t are possible if the PCL thickness d is increased so that optical tunneling of the s polarization is suppressed. However, higher values of d pose a technical challenge in device fabrication as the aspect ratio $\frac{d}{f\Lambda}$ of

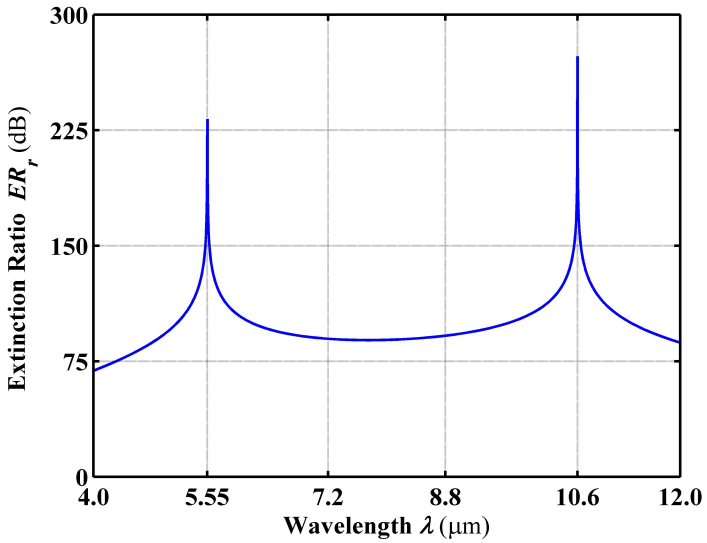

Figure 4.6: Extinction ratio in reflection ER_r as a function of the wavelength λ at the prism(ZnS)-PCL(ZnTe) interface, with angle of incidence $\phi = 45^o$ and grating period $\Lambda = 1$ μm at filling factor $f = 0.6042$.

the grating ridges increases.

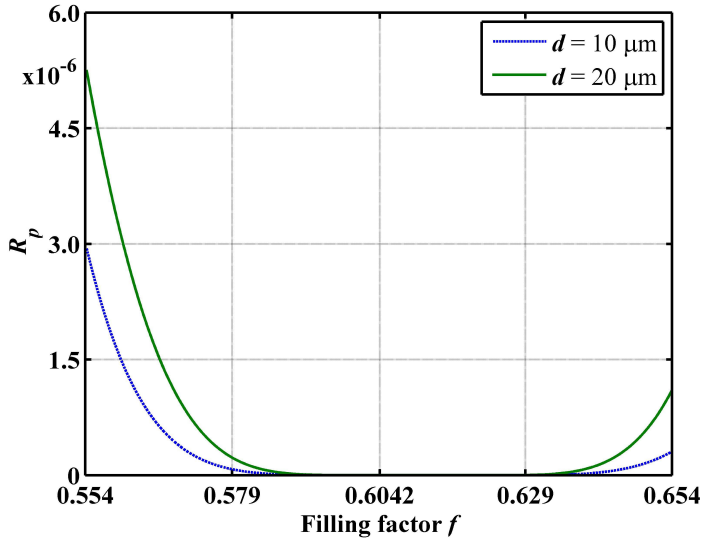

Figure 4.7: Intensity reflectance R_p of p polarization as a function of the filling factor f for ZnTe PCL embedded in ZnS prism, for layer thicknesses $d = 10$ μm and $d = 20$ μm, with angle of incidence $\phi = 45^o$ and grating period $\Lambda = 1$ μm at wavelength $\lambda = 10.6$ μm.

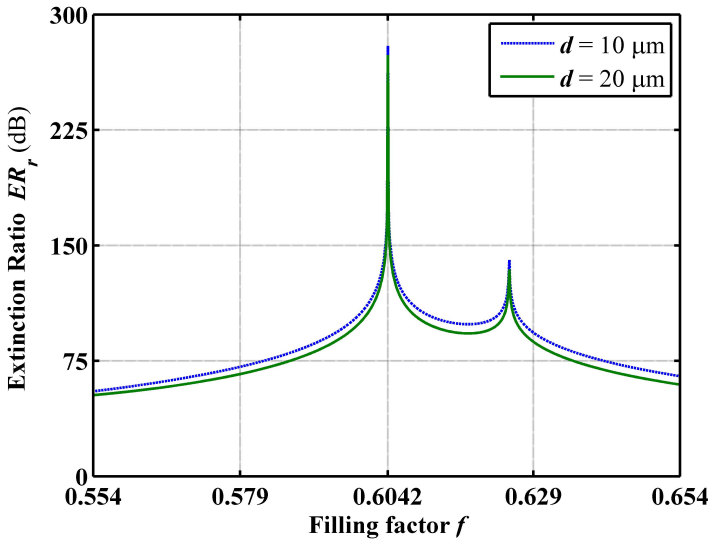

Figure 4.8: Extinction ratio in reflection ER_r as a function of the filling factor f for ZnTe PCL embedded in ZnS prism, for layer thicknesses $d = 10$ μm and $d = 20$ μm , with angle of incidence $\phi = 45^o$ and grating period $\Lambda = 1$ μm at wavelength λ=10.6 μm.

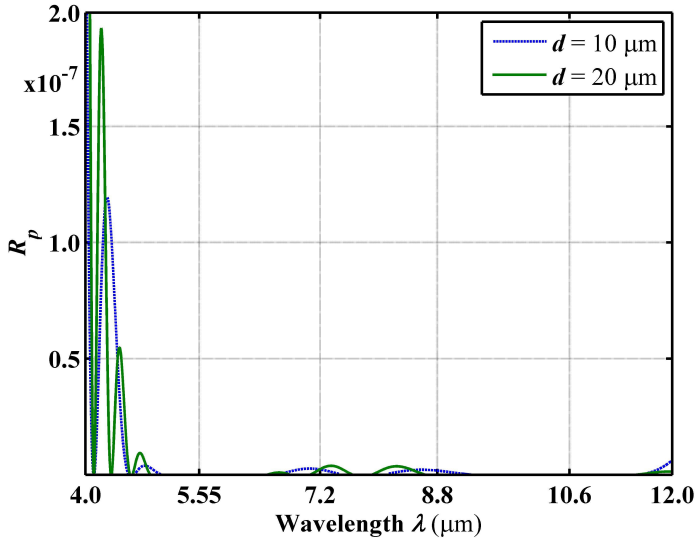

Figure 4.9: Intensity reflectance R_p of p polarization as a function of the wavelength λ for ZnTe PCL embedded in ZnS prism, for layer thicknesses $d = 10$ μm and $d = 20$ μm ,with angle of incidence $\phi = 45^o$ and grating period $\Lambda = 1$ μm at filling factor $f = 0.6042$.

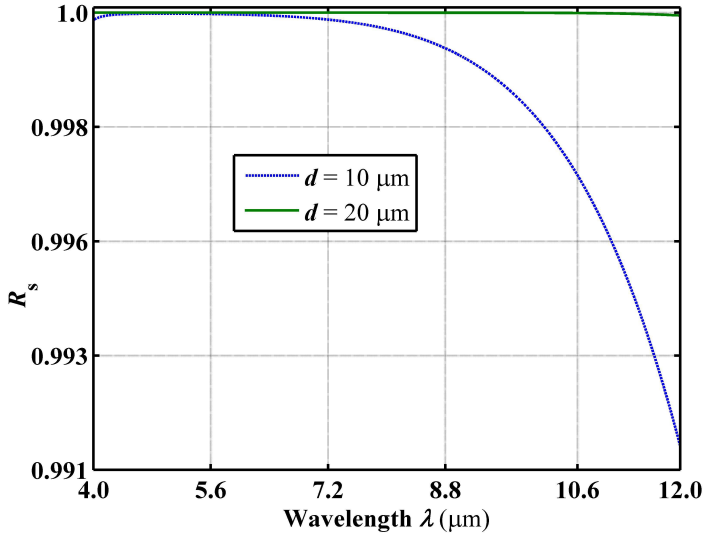

Figure 4.10: Intensity reflectance R_s of s polarization as a function of the wavelength λ for ZnTe PCL embedded in ZnS prism, for layer thicknesses $d = 10$ μm and $d = 20$ μm ,with angle of incidence $\phi = 45^o$ and grating period $\Lambda = 1$ μm at filling factor $f = 0.6042$.

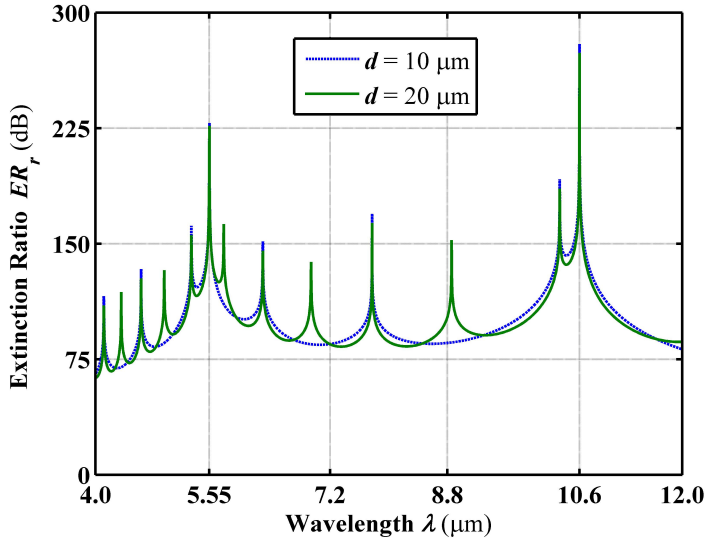

Figure 4.11: Extinction ratio in reflection ER_r as a function of the wavelength λ for ZnTe PCL embedded in ZnS prism, for layer thicknesses $d = 10$ μm and $d = 20$ μm, with angle of incidence $\phi = 45^o$ and grating period $\Lambda = 1$ μm at filling factor $f = 0.6042$.

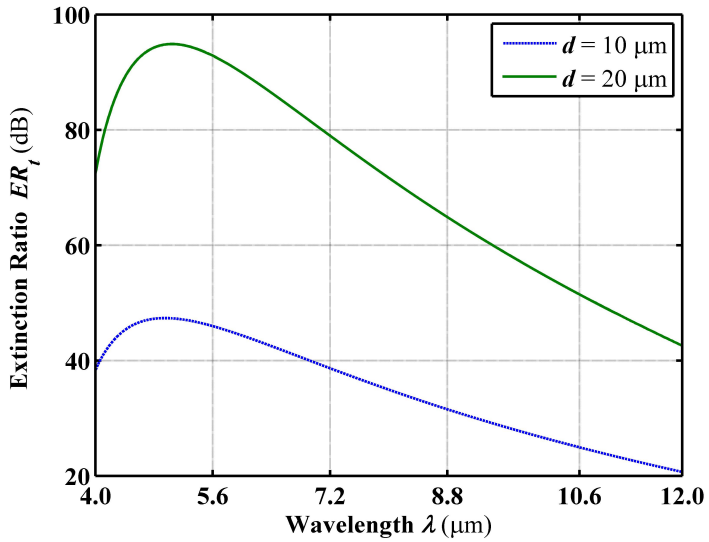

Figure 4.12: Extinction ratio in transmission ER_t as a function of the wavelength λ for ZnTe PCL embedded in ZnS prism, for layer thicknesses $d = 10$ μm and $d = 20$ μm, with angle of incidence $\phi = 45^o$ and grating period $\Lambda = 1$ μm at filling factor $f = 0.6042$.

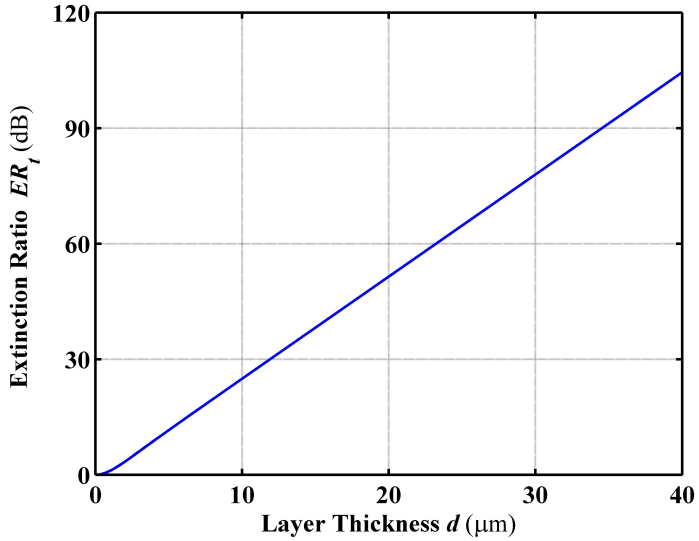

Figure 4.13: Extinction ratio in transmission ER_t as a function of 1-D (ZnTe)PCL thickness d, with angle of incidence $\phi = 45^o$, grating period $\Lambda = 1\mu$m, and wavelength $\lambda = 10.6$ μm at filling factor $f = 0.6042$.

Chapter 5

Broadband IR PBS Using Ge Photonic-Crystal Layer Embedded in Si Cube

5.1 Introduction

A PBS design of Ge-Si materials is achieved by following the iterative steps of the the design procedure of Fig. 3.2 for the same parameters (grating period Λ=1 μm and wavelength λ=10.6 μm) used in Chapter 4 and n_c(Ge)=4.0030 [70]. By using $x = 0.5188$, we obtain $\phi_{cs} = 31.2528^o$, $f = 0.6908$, $n_e = 1.7731$, and $n_o = 3.4176$. $\Delta n = n_e - n_o = -1.6445$ which represents giant birefringence for Ge PCL. For index matching ($n_o = n$) Si is chosen as a prism which has a refractive index of n(Si)=3.4176 [70] at λ=10.6 μ m The parameters for 1-D Ge(PCL) embedded in Si(cube prism) are summarized in Table 5.1.

5.2 Non-Interference Photonic-Crystal Layer of Ge Embedded in Si Cube

Table 5.1: Design parameters for PBS using Ge PCL with grating period $\Lambda = 1$ μm embedded in ZnS cube at wavelength λ=10.6 μm

n_c(Ge)	f	n_e	n_o	n(Si)	ϕ_{cs}
4.0030	0.6908	1.7731	3.4176	3.4176	31.2528^o

Figure 5.1 shows the intensity reflectance R_s of s polarization at the prism(SI)-PCL(Ge) interface as a function of angle of incidence ϕ using Eq. (4.2), with all other parameters kept

constant ($\Lambda = 1\mu$m, filling factor $f = 0.6908$, and wavelength $\lambda = 10.6$ μm). As shown in Fig. 5.1 the critical angle $\phi_{cs} = 31.2528^o$ is $\approx 14^o$ away from the design angle of incidence $\phi = 45^o$, which gives an internal field of view (FOV) of $\pm 14^o$ and corresponding external (in-air) FOV of 47^o.

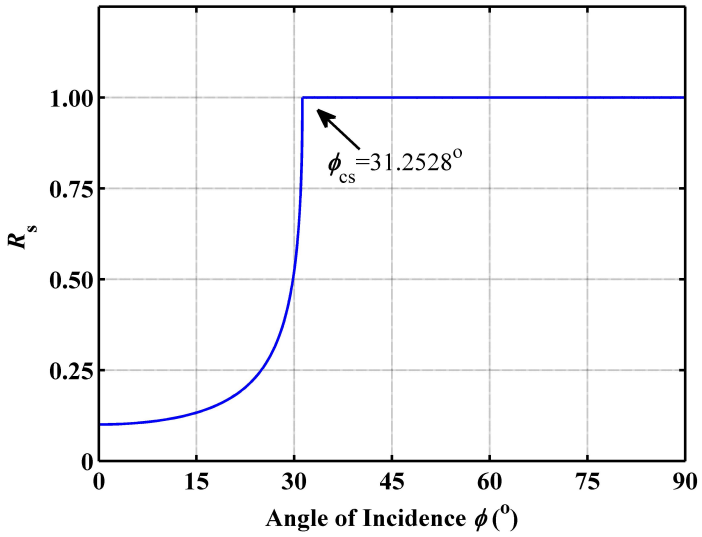

Figure 5.1: Intensity reflectance R_s of s polarization as a function of the angle of incidence ϕ at the prism(Si)-PCL(Ge) interface, with and grating period $\Lambda = 1$ μm and filling factor $f = 0.6908$ at wavelength $\lambda = 10.6$ μm.

Figure 5.2 shows the intensity reflectance R_p of p polarization versus the filling factor f as it is changed by $\approx \pm 9\%$ around the design value $f = 0.6908$, with all other parameters kept constant. $R_p < 1.1 \times 10^{-6}$ over the entire change of the filling factor $0.6408 \leq f \leq 0.7408$, which indicates the p polarization component is almost totally transmitted.

Figure 5.3 shows the extinction ratio in reflection ER_r versus the filling factor f as it is changed by $\approx \pm 9\%$ around the design value $f = 0.6908$, with all other parameters kept constant. Figure 5.3 has a spike $ER_r \approx 233$dB at the design filling factor $f = 0.6908$ which drops to $ER_r \approx 56$ dB as the filling factor ranged from 0.6408 to 0.7408. This indicates good tolerance to small dimensional errors.

Figure 5.4 shows the deviation from index matching of p-polarized light (i.e., $n_o = n$) as the wavelength λ is varied $4 \leq \lambda \leq 12$ μm for the Si prism and Ge PCL, with all other

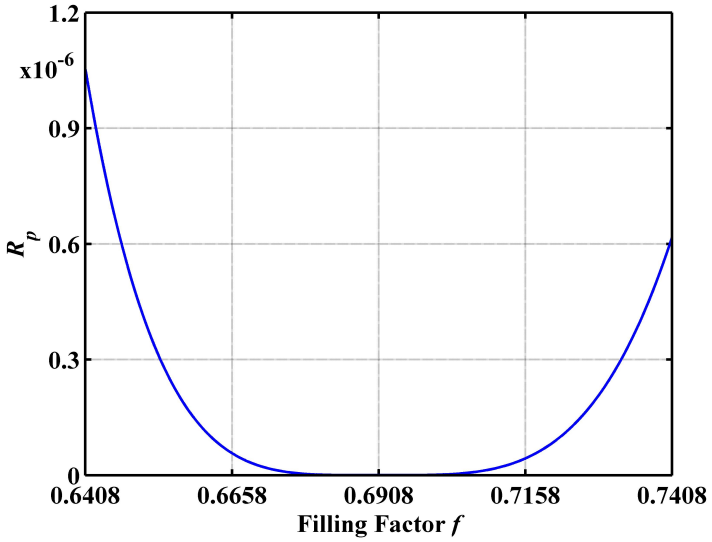

Figure 5.2: Intensity reflectance R_p of p polarization at the prism(Si)-PCL(Ge) interface as a function of the filling factor f , with angle of incidence $\phi = 45^o$ and grating period $\Lambda = 1$ μm at wavelength $\lambda = 10.6$ μm.

parameters kept constant. Refractive index matching occurs between $n_o = n$ at the design wavelength λ=10.6 μm, The dispersion of the coating and prism materials is considered [70], and unity intensity reflectance of s polarization ($R_s = 1$) is maintained over the entire bandwidth $4 \leq \lambda \leq 12$ μm.

Figure 5.5 shows the intensity reflectance R_p of p polarization as a function of the wavelength λ, for $4 \leq \lambda \leq 12$ μm, with all other parameters kept constant. The minimum reflection of p polarization $R_p \approx 0$ occurs at the design wavelength λ=10.6 μm which is consistent with Fig. 5.4. The maximum intensity reflectance R_p is $< 2.6 \times 10^{-5}$ for the entire bandwidth $4 \leq \lambda \leq 12$ μm.

Figure 5.6 shows the extinction ratio in reflection ER_r as a function of the wavelength λ, for $4 \leq \lambda \leq 12$ μm, with all other parameters kept constant. Notice that the ER_r is $>$ 45 dB over the full spectral range and spikes at the design wavelength $\lambda = 10.6$ μm which is consistent with Figs. 5.4 and 5.5. Therefore near-ideal broadband polarization on reflection is possible.

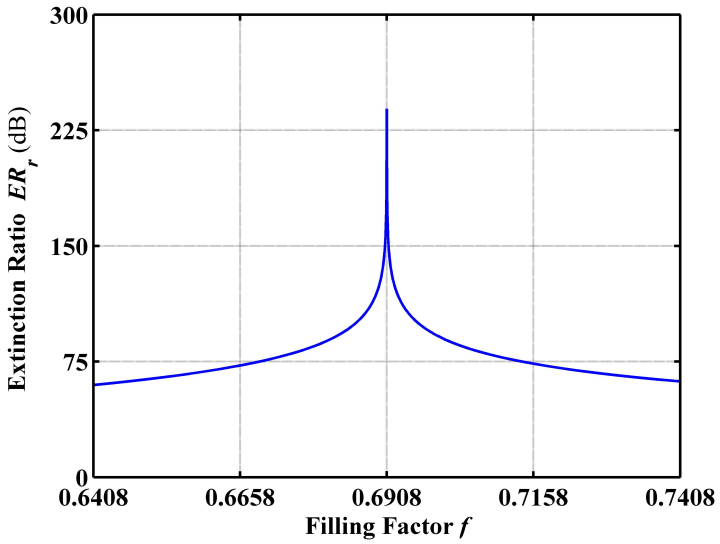

Figure 5.3: Extinction ratio in reflection ER_r versus the filling factor f at the prism(Si)-PCL(Ge) interface, with angle of incidence $\phi = 45^o$, grating period $\Lambda = 1$ μm, and wavelength $\lambda = 10.6$ μm.

5.3 Interference Effects within the Photonic-Crystal Layer of Ge Embedded in Si Cube

In this section we consider the effects of the interference in PCL with two different thicknesses d=10 μm and d=20 μm, then the performance of the PBS is calculated and compared for both thicknesses.

Figure 5.7 shows the intensity reflectance R_p of p polarization as a function of the filling factor f at the prism(Si)-PCL(Ge) interface for thicknesses $d = 10$ μm and $d = 20$ μm, with all other parameters kept constant. $R_p \approx 0$ for both designs at the design filling factor $f = 0.6908$, however, the design with $d = 10$ μm show a smaller reflection as f is away from the design point which is consistent with Fig. 5.2.

Figure 5.8 shows extinction ratio in reflection ER_r as a function of the filling factor f for Ge PCL embedded in Si prism, for layer thicknesses $d = 10$ μm and $d = 20$ μm, with all other parameters kept constant. As expected, a spike appears at the design point $f = 0.6908$ for both designs, and another spike appears at $f = 0.6799$ for the design of layer thickness of $d = 20$ μm.

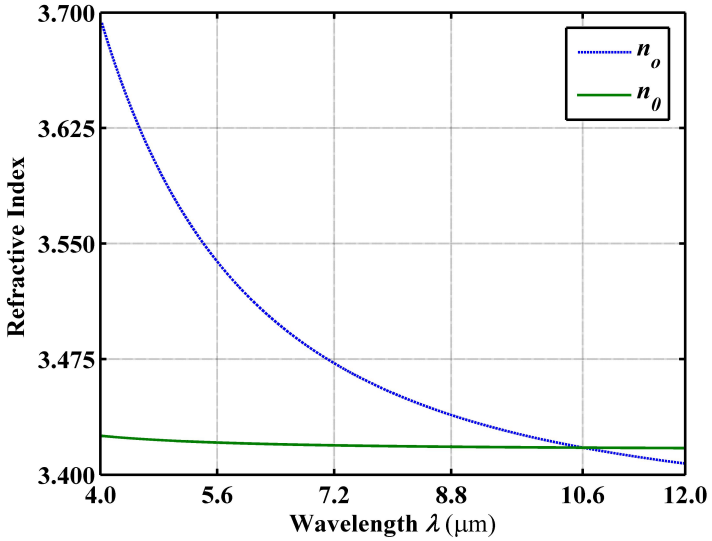

Figure 5.4: Deviation from index matching of p–polarized light as the wavelength λ is varied $4 \leq \lambda \leq 12$ μm for the Si prism and Ge PCL at angle of incidence $\phi = 45^o$, grating period $\Lambda = 1$ μm, and takes into account dispersion of the optical properties of Ge and Si.

Figure 5.9 shows the intensity reflectance R_p of p polarization as a function of the wavelength λ, for $4 \leq \lambda \leq 12$ μm at the prism(Si)-PCL(Ge) interface for layer thicknesses $d = 10$ μm and $d = 20$ μm, with all other parameters kept constant. The interference oscillations of R_p are less than 1×10^{-4} over the entire wavelength range. Excellent performance is maintained when interference effects in the PCL are taken into consideration.

The intensity reflectance R_s of s polarization as a function wavelength λ for Ge PCL embedded in Si prism, for layer thicknesses $d = 10$ μm and $d = 20$ μm, is very close to unity reflection $R_s = 1$, with a deviation from unity less than 1×10^{-6} and 4×10^{-15} for the designs with layer thicknesses $d = 10$ μm and $d = 20$ μm, respectively.

Figure 5.10 shows the extinction ratio in reflection ER_r as a function of the wavelength λ, for $4 \leq \lambda \leq 12$ μm for Ge PCL embedded in Si prism, for layer thicknesses $d = 10$ μm and $d = 20$ μm, with all other parameters kept constant. Multiple spikes appear and reach maximum at the design point λ=10.6 μm which is correspond and consistent with $R_p = 0$ of Fig. 5.9.

Figure 5.11 shows the extinction ratio in transmission ER_t as a function of the wavelength

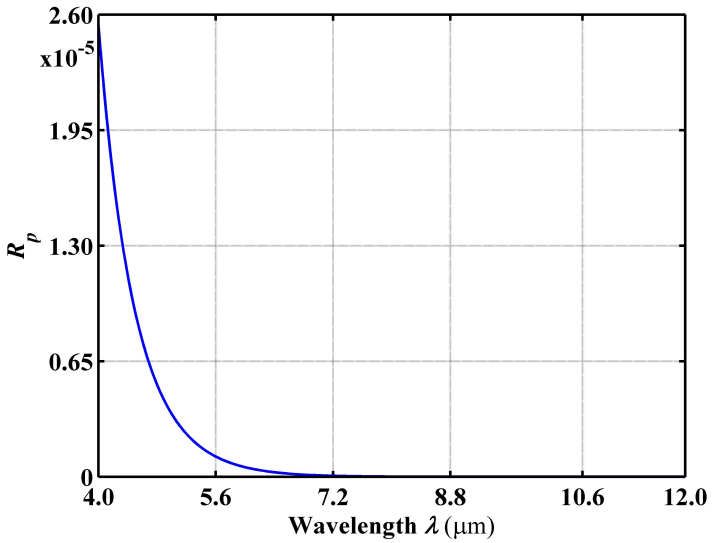

Figure 5.5: Intensity reflection R_p of p polarization as a function of the wavelength λ at the prism(Si)-PCL(Ge) interface, with angle of incidence $\phi = 45^o$ and grating period $\Lambda = 1$ μm at filling factor $f = 0.6908$.

λ, for $4 \leq \lambda \leq 12$ μm for Ge PCL embedded in Si prism, for layer thickness $d = 10$ μm, with all other parameters kept constant. $ER_t > 100$ dB is achieved for $4 \leq \lambda \leq 8$ μm with maximum near λ=4.8 μm followed by monotonic drop at longer wavelengths. This behavior is consistent with the decrease of R_s as $\frac{d}{\lambda}$ decreases caused by increased optical tunneling.

Figure 5.12 shows the extinction ratio in transmission as a function of the layer thickness d at the prism(Si)-PCL(Ge) interface, with all other parameters kept constant. Higher values of ER_t are possible if the PCL thickness d is increased so that optical tunneling of the s polarization is suppressed. However, higher values of d pose a technical challenge in device fabrication as the aspect ratio $\frac{d}{f\Lambda}$ of the grating ridges increases.

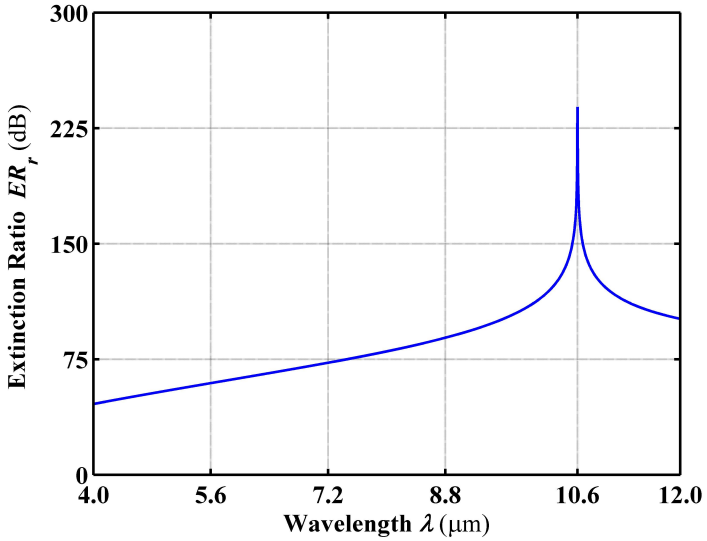

Figure 5.6: Extinction ratio in reflection ER_r as a function of the wavelength λ at the prism(Si)-PCL(Ge) interface, with angle of incidence $\phi = 45^o$ and grating period $\Lambda = 1$ μm at filling factor $f = 0.6908$.

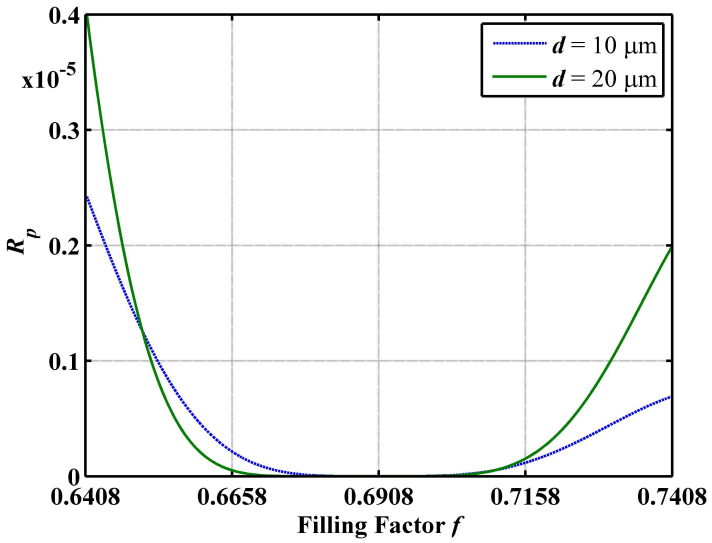

Figure 5.7: Intensity reflection R_p of p polarization as a function of the filling factor f at the prism(Si)-PCL(Ge) interface for layer thicknesses $d = 10$ μm and $d = 20$ μm, with angle of incidence $\phi = 45^o$ and grating period $\Lambda = 1$ μm at wavelength $\lambda = 10.6$ μm.

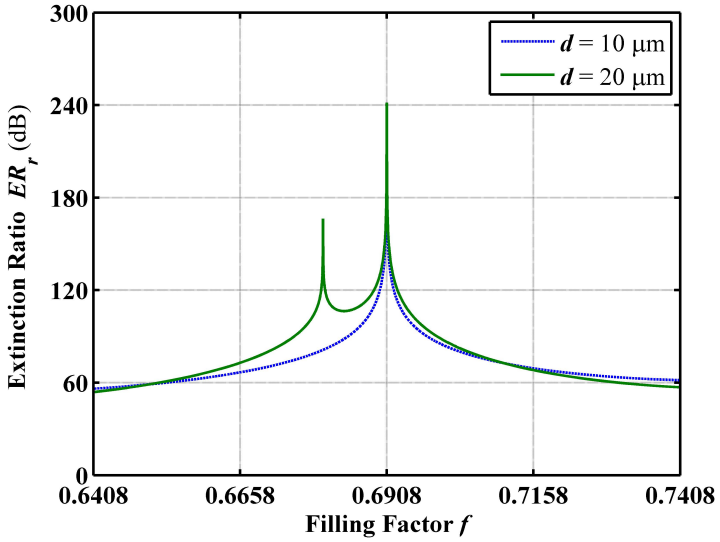

Figure 5.8: Extinction ratio in reflection ER_r as a function of the filling factor f for Ge PCL embedded in Si prism, for layer thicknesses $d = 10$ μm and $d = 20$ μm, with angle of incidence $\phi = 45^o$ and grating period $\Lambda = 1$ μm at wavelength λ=10.6 μm.

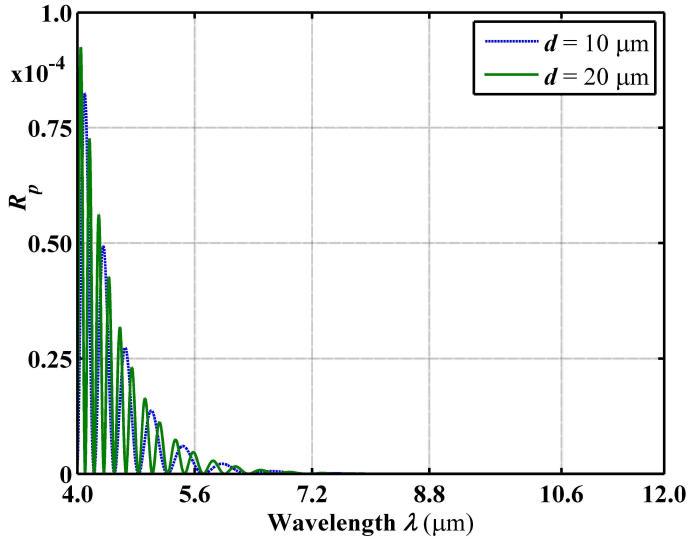

Figure 5.9: Intensity reflection R_p of p polarization as a function of the wavelength λ for Ge PCL embedded in Si prism, for layer thicknesses $d = 10$ μm and $d = 20$ μm,with angle of incidence $\phi = 45^o$ and grating period $\Lambda = 1$ μm at filling factor $f = 0.6908$.

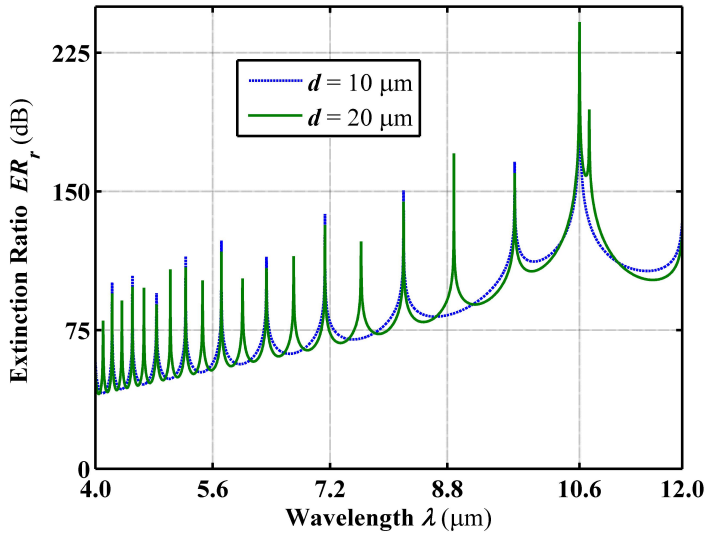

Figure 5.10: Extinction ratio in reflection ER_r as a function of the wavelength λ for Ge PCL embedded in Si prism, for layer thicknesses $d = 10$ μm and $d = 20$ μm, with angle of incidence $\phi = 45^o$ and grating period $\Lambda = 1$ μm at filling factor $f = 0.6908$.

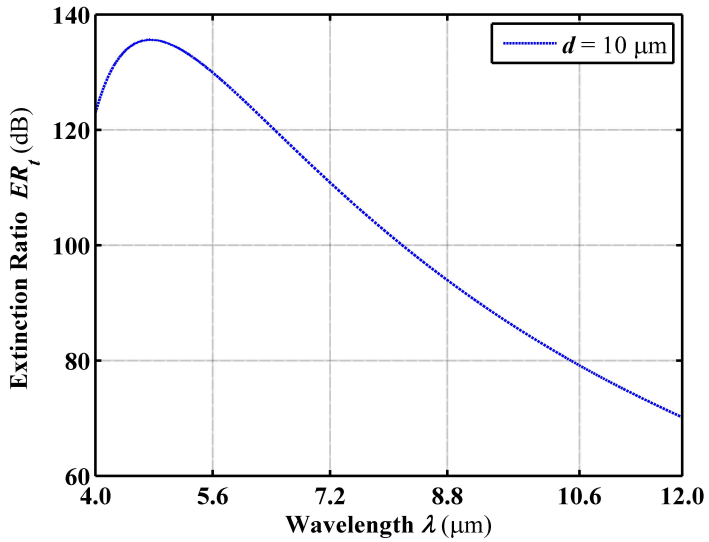

Figure 5.11: Extinction ratio in transmission ER_t as a function of the wavelength λ for Ge PCL embedded in Si prism, for layer thicknesses $d = 10$ μm and $d = 20$ μm, with angle of incidence $\phi = 45^o$ and grating period $\Lambda = 1$ μm at filling factor $f = 0.6908$.

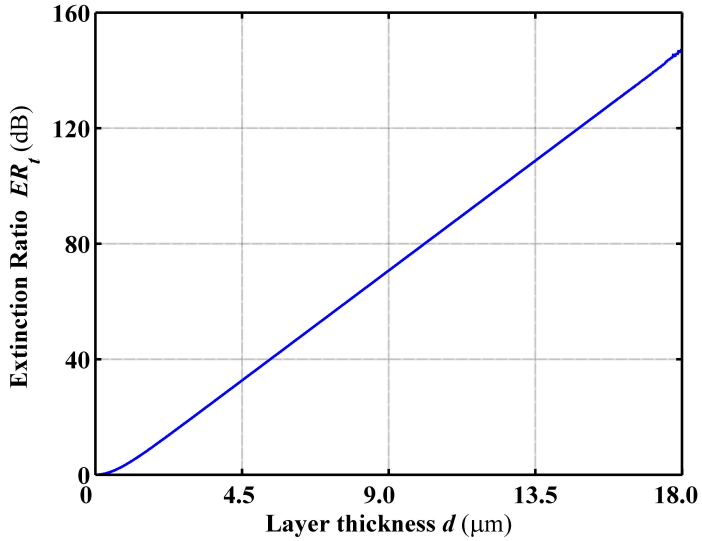

Figure 5.12: Extinction ratio in transmission ER_t as a function of 1-D (Ge)PCL thickness d, with angle of incidence $\phi = 45^o$, grating period $\Lambda = 1\mu$m, and wavelength $\lambda = 10.6$ μm at filling factor $f = 0.6908$.

Chapter 6

Visible Spectrum PBS Using ZnTe PCL Embedded ZnS Cube

6.1 Introduction

PBS design that uses ZnTe 1-D PCL (grating), which is embedded between two right-angle ZnS prisms, is presented for the He–Ne laser wavelength $\lambda = 633$ nm, a grating period $\Lambda = 100$ nm, and $n_c(\text{ZnTe}) = 2.9886$ [70]. By applying the iterative steps of the design procedure shown in Fig. 3.2 and using $x = 0.6062$, we obtain $\phi_{cs} = 37.3152^o$, $f = 0.5299$, $n_o = 2.3503$, $n_e = 1.42476$. This represents a PCL with giant negative birefringence $\Delta n = n_e - n_o = -0.9256$. For index matching of n_o and n ZnS, is chosen as a prism which has a refractive index of $n = 2.3503$ at λ =633 nm [70]. Design parameters for a PBS using ZnTe PCL embedded in a ZnS cube at wavelength 633 nm are listed in Table 6.1.

6.2 Non-Interference Photonic-Crystal Layer of ZnTe Embedded in ZnS Cube

Table 6.1: Design parameters for PBS using ZnTe PCL with grating period $\Lambda = 100$ nm embedded in ZnS cube at wavelength λ=633 nm

n_c(ZnTe)	f	n_e	n_o	n(ZnS)	ϕ_{cs}
2.9886	0.5299	1.4247	2.3503	2.3503	37.3152^o

Figure 6.1 shows the intensity reflectance R_s of s polarization as a function of angle of incidence ϕ at the prism(ZnS)-PCL(ZnTe) interface using Eq. (4.2), with grating period

$\Lambda = 100$ nm and filling factor $f = 0.5299$ at wavelength $\lambda = 10.6$ μm. As shown in Fig. 6.1, the critical angle $\phi_{cs} = 37.3152^o$ is 7^o away from the design angle of incidence $\phi = 45^o$ which gives an internal field of view (FOV) of $\pm 7^o$ and a corresponding external (in-air) FOV of $\pm 18^o$.

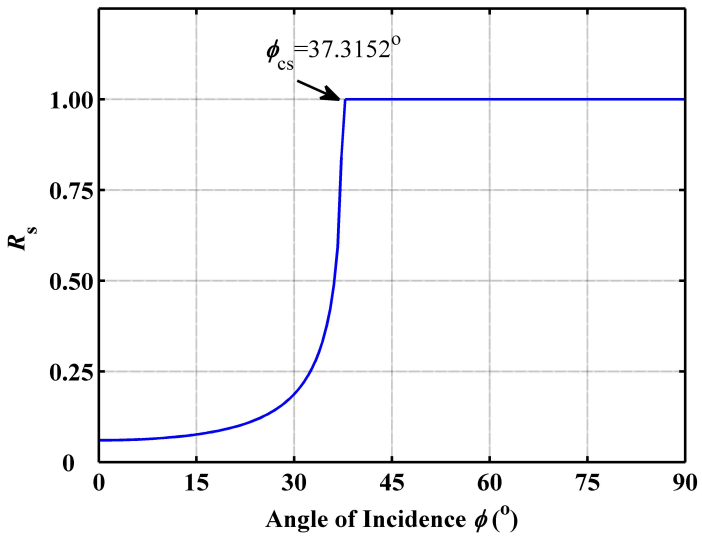

Figure 6.1: Intensity reflection R_s of s polarization as a function of the angle of incidence ϕ at the prism(ZnS)-PCL(ZnTe) interface, with grating period Λ=100 nm and filling factor $f = 0.5299$ at wavelength $\lambda = 633$ nm.

Figure 6.2 shows the intensity reflectance R_p of p polarization versus the filling factor f as it is changed by $\approx \pm 9\%$ around the design value $f = 0.5299$, with all other parameters kept constant. This reflection is very small, $R_p < 2.4 \times 10^{-6}$. On the other hand, the s polarization is not affected by this change of filling factor $0.4799 \leq f \leq 0.5799$ and maintains unity intensity reflectance ($R_s = 1$).

Figure 6.3 shows the extinction ratio in reflection ER_r versus the filling factor f as it is changed by $\approx \pm 9\%$ around the design value $f = 0.5299$, with all other parameters kept constant. Figure 6.3 has a spike at the design value $f = 0.5299$ and $ER_r > 56$ dB as the filling factor is changed $0.4799 \leq f \leq 0.5799$; this indicates good tolerance to small dimensional errors.

Figure 6.4 shows the deviation from index matching of p–polarized light (i.e., $n_o = n$)

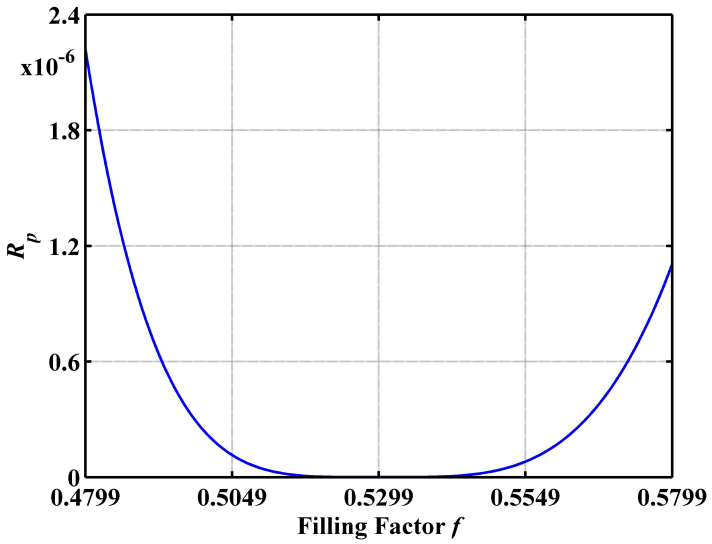

Figure 6.2: Intensity reflection R_p of p polarization as a function of the filling factor f at the prism(ZnS)-PCL(ZnTe) interface, with angle of incidence $\phi = 45^o$ and grating period $\Lambda = 100$ nm at wavelength $\lambda = 633$ nm.

as the wavelength is varied $552 \leq \lambda \leq 713$ nm for a ZnS prism and a ZnTe PCL, with all other parameters kept constant. Index matching ($n_o = n$) occurs at the design wavelength $\lambda = 633$ nm. The dispersion of the coating and prism materials is considered [70], and the unity intensity reflectance of the s polarization ($R_s = 1$) is maintained for the entire bandwidth $553 \leq \lambda \leq 713$ nm.

Figure 6.5 shows the intensity reflectance R_p of the p polarization as a function of the wavelength λ, for $553 \leq \lambda \leq 713$ nm, with all other parameters kept constant. The minimum reflectance of p polarization (maximum transmission) $R_p \approx 0$ takes place at the design wavelength $\lambda = 633$ nm, which is consistent with Fig. 6.4. The maximum intensity reflectance R_p is $< 5 \times 10^{-6}$ for the entire bandwidth $553 \leq \lambda \leq 713$ nm.

Figure 6.6 shows the extinction ratio in reflection ER_r as a function of the wavelength λ, for $553 \leq \lambda \leq 713$ nm, with all other parameters kept constant. Notice that the ER_r is > 53 dB over the full spectral range and spikes at design wavelength $\lambda = 633$ nm which is consistent with Figs. 6.4 and 6.5.

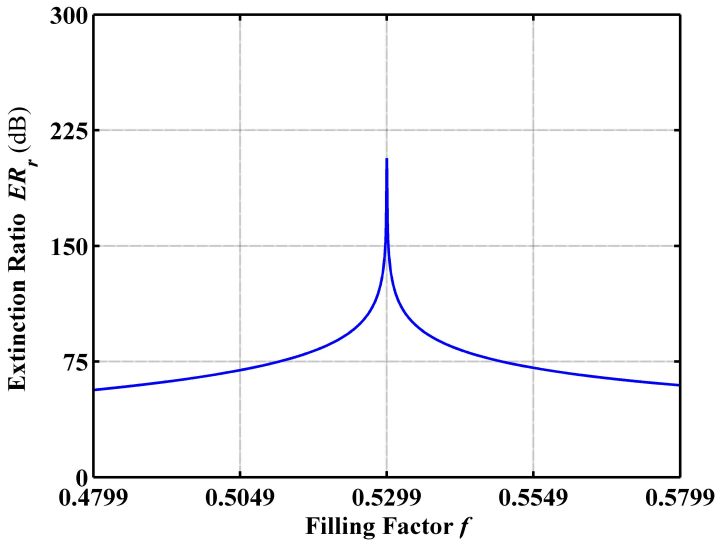

Figure 6.3: Extinction ratio in reflection ER_r versus the filling factor f at the prism(ZnS)-PCL(ZnTe) interface, with angle of incidence $\phi = 45^o$ and grating period $\Lambda = 100$ nm at wavelength $\lambda = 633$ nm.

6.3 Interference Effects within the Photonic-Crystal Layer of ZnTe Embedded in ZnS Cube

In the previous section the effects of the interference were ignored and the thickness of the layer d assumed to be larger than the penetration depth of the s polarization component wave. In this section the PCL with two different thicknesses, d=600 nm and d=1200 nm, is considered. The performance of the PBS is calculated and compared for both thicknesses.

Figure 6.7 shows the intensity reflectance R_p of p polarization as a function of the filling factor f at the prism(ZnS)-PCL(ZnTe) interface of thicknesses $d = 600$ nm and $d = 1200$ nm, with all other parameters kept constant. $R_p \approx 0$ for both designs at the design filling factor $f = 0.5299$. The design with $d = 600$ nm shows a smaller reflection as f is away from the design point, which is consistent with Fig. 6.2.

Figure 6.8 shows extinction ratio in reflection ER_r as a function of the filling factor f at the prism(ZnS)-PCL(ZnTe) interface for layer thicknesses $d = 600$ nm and $d = 1200$ nm, with all other parameters kept constant. As expected a spike appears at the design point

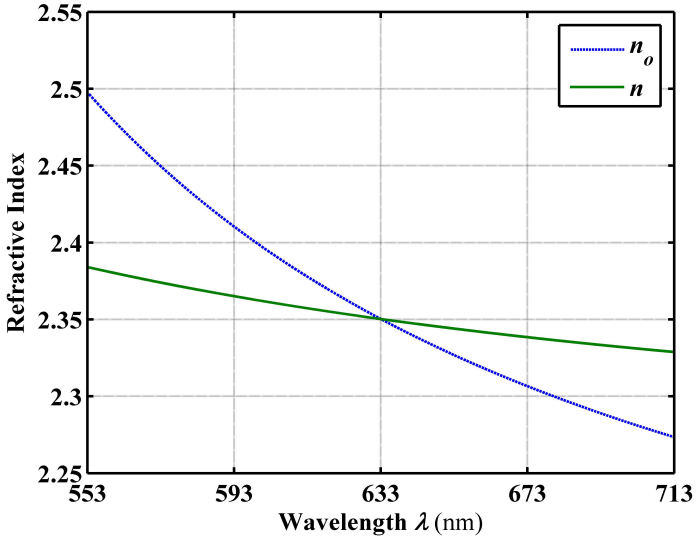

Figure 6.4: Deviation from index matching of p–polarized light as the wavelength is varied $553 \leq \lambda \leq 713$ nm for the prism of ZnS and and PCL of ZnTe, with angle of incidence $\phi = 45^o$, grating period $\Lambda = 100$ nm, and taking into account the dispersion of the optical properties of ZnTe and ZnS.

$f = 0.5299$ and there is another one at $f = 0.4971$.

Figure 6.9 shows the intensity reflectance R_p of p polarization as a function of the wavelength λ, for $553 \leq \lambda \leq 713$ nm at the prism(ZnS)-PCL(ZnTe) interface for layer thicknesses $d = 600$ nm and $d = 1200$ nm, with all other parameters kept constant. The interference oscillations of R_p are all less than 5×10^{-6}. Excellent performance is maintained when interference effects in the PCL are taken into consideration.

Figure 6.10 shows the intensity reflectance R_s of the s polarization as a function of wavelength λ for layer thickness $d = 600$ nm, with all other parameters kept constant. R_s falls off monotonically as λ increases and d decreases, which is consistent with the expected increase in optical tunneling as $\frac{d}{\lambda}$ decreases. The intensity reflectance R_s for the design layer thickness $d = 1200$ nm is very close to unity reflection $R_s = 1$, with deviation from unity being $< 4 \times 10^{-8}$ for the entire bandwidth $553 \leq \lambda \leq 713$ nm.

Figure 6.11 shows the the extinction ratio in reflection ER_r as a function of the wavelength Λ, for $553 \leq \lambda \leq 713$ nm, for layer thicknesses $d = 600$ nm and $d = 1200$ nm, with all

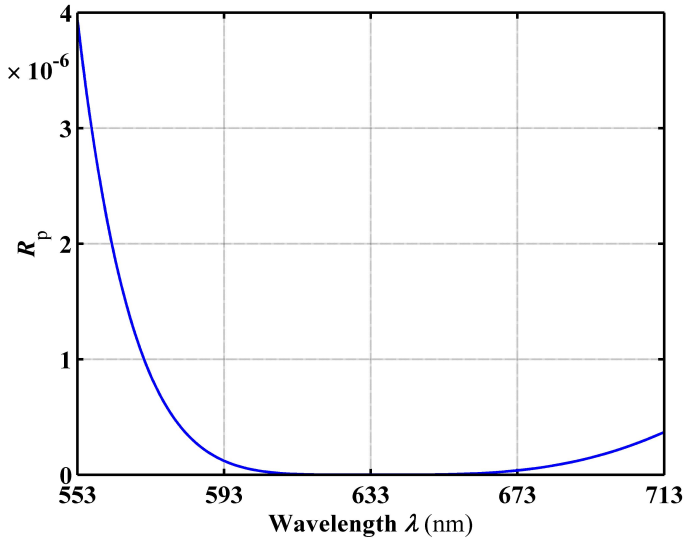

Figure 6.5: Intensity reflection R_p of p polarization as a function of the wavelength λ at the prism(ZnS)-PCL(ZnTe) interface, with angle of incidence $\phi = 45^o$ and grating period $\Lambda = 100$ nm at filling factor $f = 0.5299$.

other parameters kept constant. Multiple spikes appear that correspond to $R_p = 0$ in Fig. 6.9. $ER_r > 60$ dB is achieved over the entire bandwidth $553 \leq \lambda \leq 713$ nm and indicates near–ideal polarization on reflection.

Figure 6.12 shows extinction ratio in transmission ER_t as a function of the wavelength λ, for $553 \leq \lambda \leq 713$ nm, for layer thicknesses $d = 600$ nm and $d = 1200$ nm, with all other parameters kept constant. Both designs show ER_t as a decreasing linear function of λ. This behavior is consistent with the decrease of R_s as $\frac{d}{\lambda}$ decreases, caused by increased optical tunneling.

Figure 6.13 shows the extinction ratio in transmission ER_t as a function of the layer thickness d, with all other parameters kept constant. Higher values of ER_t are possible if the PCL thickness d is increased so that optical tunneling of the s polarization is suppressed.

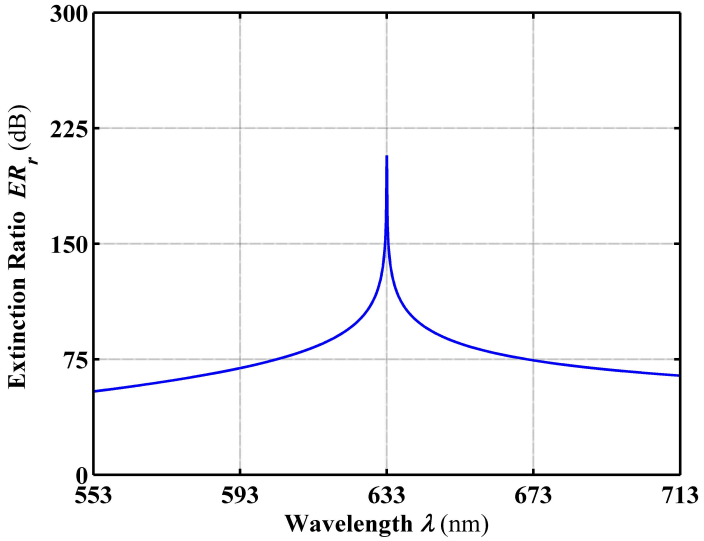

Figure 6.6: Extinction ratio in reflection ER_r as a function of the wavelength λ at the prism(ZnS)-PCL(ZnTe) interface, with angle of incidence $\phi = 45^o$, grating period $\Lambda = 100$ nm, and filling factor $f = 0.5299$.

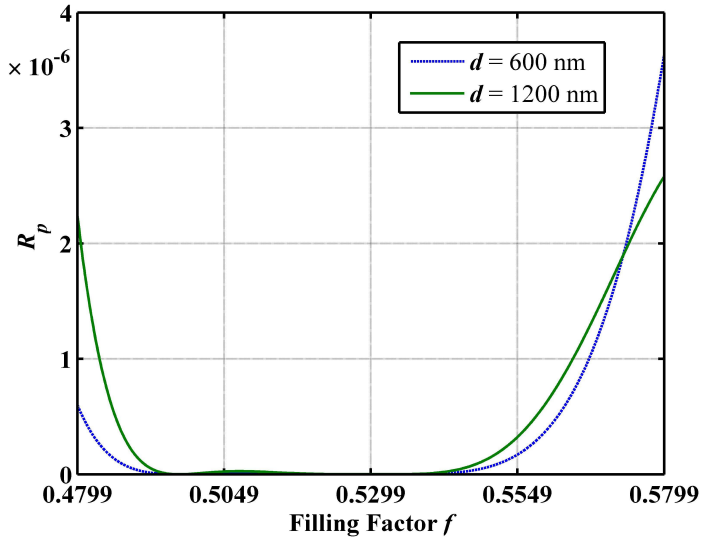

Figure 6.7: Intensity reflection R_p of p polarization as a function of the filling factor f for layer thicknesses $d = 600$ nm and $d = 1200$ nm, with angle of incidence $\phi = 45^o$, grating period $\Lambda = 100$ nm, and wavelength $\lambda = 633$ nm.

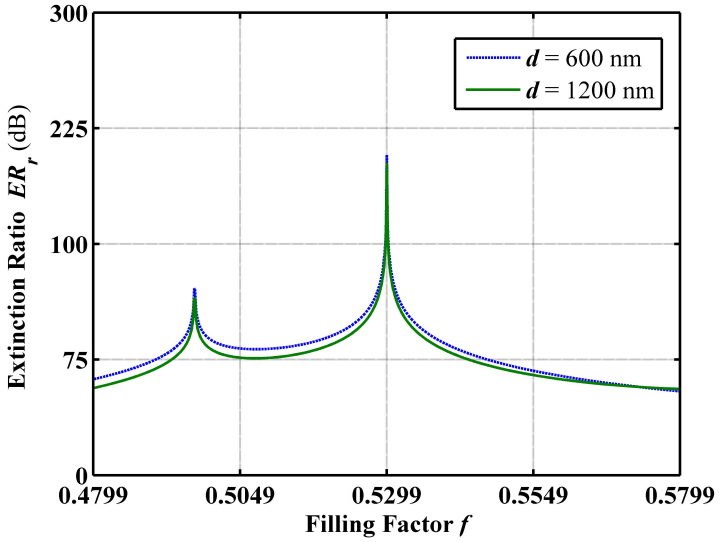

Figure 6.8: Extinction ratio in reflection ER_r as a function of the filling factor f for layer thicknesses $d = 600$ nm and $d = 1200$ nm, with angle of incidence $\phi = 45^o$ and grating period $\Lambda = 100$ nm at wavelength λ=10.6 μm.

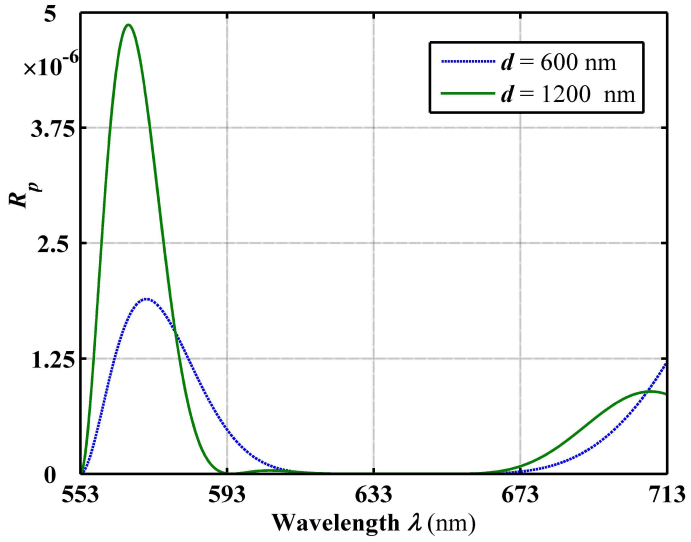

Figure 6.9: Intensity reflection R_p of p polarization as a function of the wavelength λ at for layer thicknesses $d = 600$ nm and $d = 1200$ nm, with angle of incidence $\phi = 45^o$, grating period $\Lambda = 100$ nm, and filling factor $f = 0.5299$.

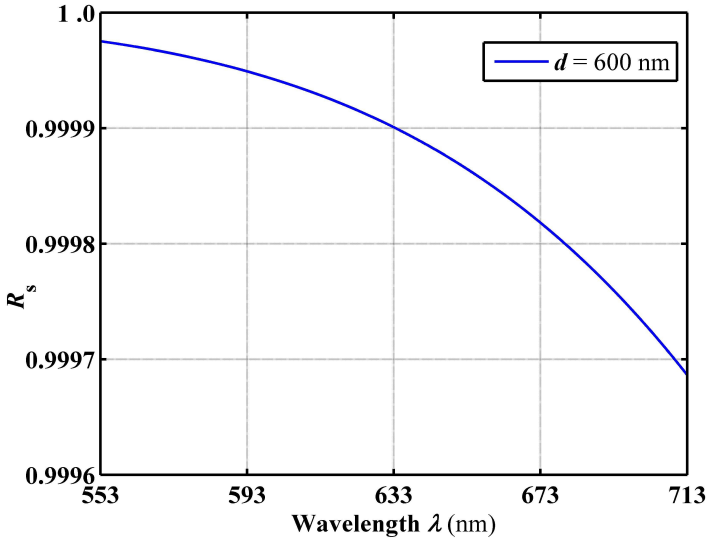

Figure 6.10: Intensity reflection R_s of s polarization as a function of the wavelength λ for layer thickness $d = 600$ nm, with angle of incidence $\phi = 45^o$ and grating period $\Lambda = 100$ nm at filling factor $f = 0.5299$.

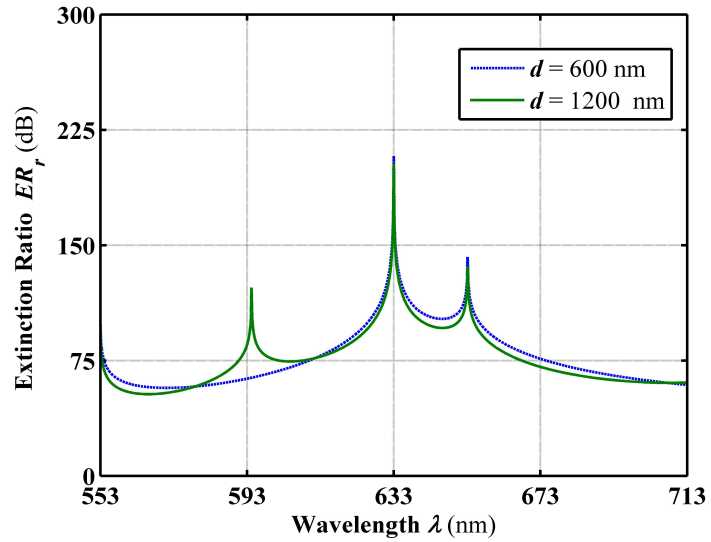

Figure 6.11: Extinction ratio in reflection ER_r as a function of the wavelength λ for layer thicknesses $d = 600$ nm and $d = 1200$ nm, with angle of incidence $\phi = 45^o$ and grating period $\Lambda = 100$ nm at filling factor $f = 0.5299$.

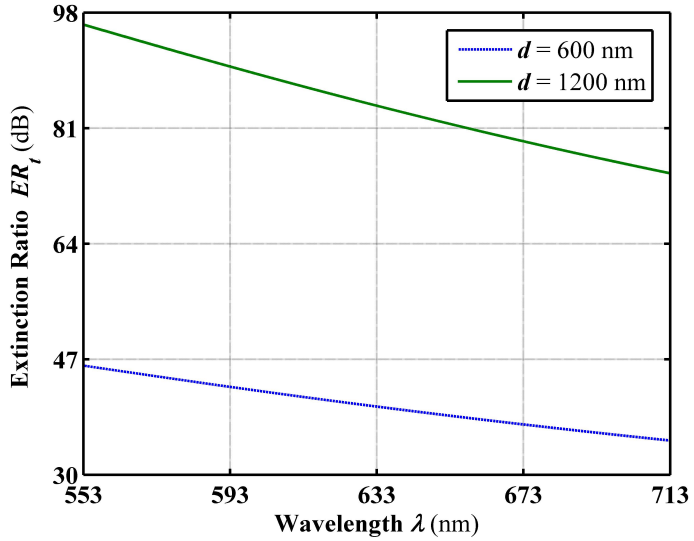

Figure 6.12: Extinction ratio in transmission ER_t as a function of the wavelength λ for layer thicknesses $d = 600$ nm and $d = 1200$ nm, with angle of incidence $\phi = 45^o$, grating period $\Lambda = 100$ nm, and filling factor $f = 0.5299$.

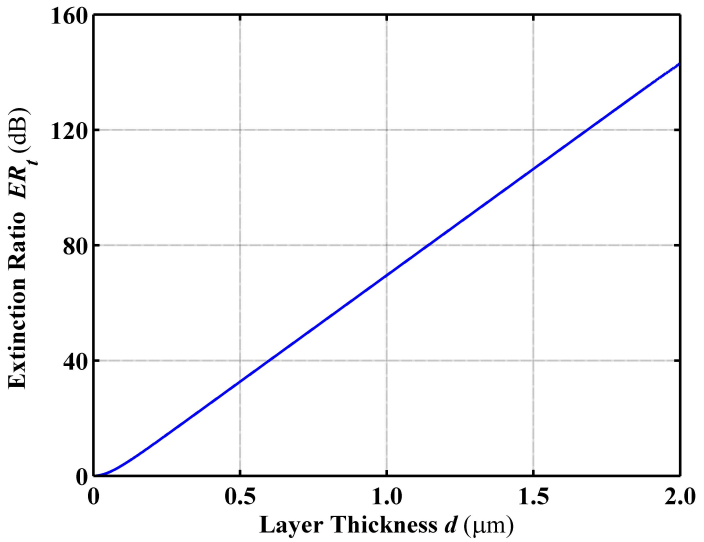

Figure 6.13: Extinction ratio in transmission ER_t as a function of thickness d of 1-D (ZnTe)PCL at angle of incidence $\phi = 45^o$, grating period $\Lambda = 100$ nm, wavelength $\lambda = 10.6$ μm and filling factor $f = 0.5299$.

Chapter 7

Circular Polarizing Beam Splitter

7.1 Introduction

Circular polarizing beam splitters (CPBS's) are used to separates a linearly polarized incoming beam into two circularly polarized beams that travel in different directions by transmission and reflection.

7.2 Design Procedure

Figure 7.1(a) shows the cross section of a 1-D PCL of thickness d that consists of a rectangular grating of coating material of refractive index n_c, grating period Λ, and filling factor f. The layer is deposited on an optically isotropic substrate (prism) of refractive index n, and the gaps between grating ridges are assumed to be filled with an isotopic material of refractive index n_f. The optic axis of the PCL is parallel to the grating vector $\overrightarrow{K}_G$. Figure 7.1(b) shows the Dual QWR PBS prism with the grating vector of the PCL normal to the plane of incidence. p and s denote the linear polarizations parallel and perpendicular to the plane of incidence, respectively.

With the $\lambda \gg \Lambda$, the PCL is equivalent to a non-diffracting homogeneous uniaxial crystal layer with its optic axis parallel to the grating vector and perpendicular to the plane

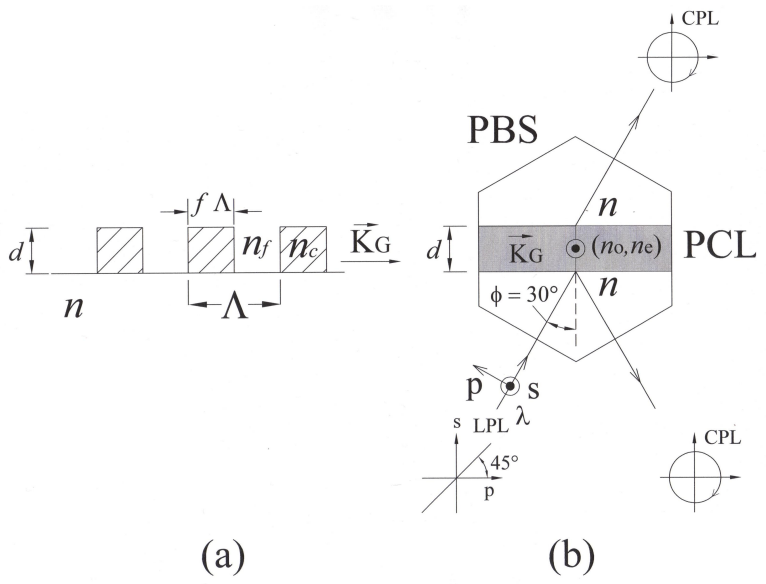

Figure 7.1: (a) Cross section of 1-D PCL of thickness d that consists of rectangular grating of a coating material of refractive index n_c, grating period Λ, and filling factor f. The layer is deposited on an optically isotropic substrate (prism) of refractive index n, and the gaps between grating ridges are assumed to be filled with isotopic material of refractive index n_f. (b) Dual QWR PBS prism with grating vector $\overrightarrow{K}_G$ of the PCL normal to the plane of incidence. p and s denote the linear polarizations parallel and perpendicular to the plane of incidence, respectively. When QWR is achieved, incident linearly polarized light (LPL) at azimuth from the plane of incidence is reflected and transmitted as circularly polarized light (CPL).

of incidence. The effective second-order ordinary n_o and extraordinary n_e are given by [69],

$$n_o^{(2)} = \left\{ (n_o^{(1)})^2 + \frac{1}{3}\left[\pi\frac{\Lambda}{\lambda}f(1-f)\right]^2 (n_c^2 - n_f^2)^2 \right\}^{\frac{1}{2}} \tag{7.1}$$

$$n_e^{(2)} = \left\{ (n_e^{(1)})^2 + \frac{1}{3}\left[\pi\frac{\Lambda}{\lambda}f(1-f)\right]^2 (\frac{1}{n_c^2} - \frac{1}{n_f^2})^2 (n_e^{(1)})^6 (n_o^{(1)})^2 \right\}^{\frac{1}{2}} \tag{7.2}$$

where

$$n_o^{(1)} = (n_f^2(1-f) + n_c^2 f)^{\frac{1}{2}}, n_e^{(1)} = (\frac{1-f}{n_f^2} + f\frac{1}{n_c^2})^{-\frac{1}{2}} \tag{7.3}$$

are the first–order indices that are independent of $\frac{\Lambda}{\lambda}$.

For an incident light beam, the change in the state of polarization in reflection and in transmission are determined by the ratios of the complex–amplitude reflection and trans-

mission coefficients for p and s polarizations:

$$\rho = \frac{r_p}{r_s} \tag{7.4}$$

$$\tau = \frac{t_p}{t_s} \tag{7.5}$$

The complex–amplitude reflection coefficients for p polarization and s polarization are given by [2]:

$$r_p = \frac{r_{01p} - r_{01p}e^{-j2\beta_p}}{1 - r_{01p}^2 e^{-j2\beta_p}} \tag{7.6}$$

$$r_s = \frac{r_{01s} - r_{01s}e^{-j2\beta_s}}{1 - r_{01s}^2 e^{-j2\beta_s}} \tag{7.7}$$

where r_{01p} and r_{01s} are prism–PCL interface reflection coefficients for p and s polarizations, respectively, given by:

$$\begin{aligned} r_{01p} &= \frac{n_o^2 \cos\phi_0 - n(n_o^2 - n^2 \sin^2\phi_0)^{\frac{1}{2}}}{n_o^2 \cos\phi_0 + n(n_o^2 - n^2 \sin^2\phi_0)^{\frac{1}{2}}} \\ r_{01s} &= \frac{n\cos\phi_0 - (n_e^2 - n^2 \sin^2\phi_0^2)^{\frac{1}{2}}}{n\cos\phi_0 + (n_e^2 - n^2 \sin^2\phi_0)^{\frac{1}{2}}} \end{aligned} \tag{7.8}$$

and the film phase thicknesses β_p and β_s are given by:

$$\begin{aligned} \beta_p &= 2\pi(\frac{d}{\lambda})(n_o^2 - n^2 \sin^2\phi_0)^2 \\ \beta_s &= 2\pi(\frac{d}{\lambda})(n_e^2 - n^2 \sin^2\phi_0)^2. \end{aligned} \tag{7.9}$$

The complex–amplitude transmission coefficients for p and s polarizations are given by [2]:

$$t_p = \frac{t_{01p}t_{12p}e^{-j\beta_p}}{1 - r_{01p}^2 e^{-j2\beta_p}} \tag{7.10}$$

$$t_s = \frac{t_{01s}t_{12s}e^{-j\beta_s}}{1 - r_{01s}^2 e^{-j2\beta_s}} \tag{7.11}$$

where t_{01p} and t_{12p} are prism–PCL interface and PCL-prism interface transmission coefficients of the p polarization, given by:

$$t_{01p} = \frac{2n\cos\phi_0}{n_o\cos\phi_0 + n(1-\frac{n^2}{n_o^2}\sin^2\phi_0)^{\frac{1}{2}}}$$
$$t_{12p} = \frac{2(n_o^2 - n\sin^2\phi_0)^{\frac{1}{2}}}{n_o\cos\phi_0 + n(1-\frac{n^2}{n_o^2}\sin^2\phi_0)^{\frac{1}{2}}} \tag{7.12}$$

and t_{01s} and t_{12s} are prism–PCL interface and PCL-prism interface transmission coefficients of the s polarization, given by:

$$t_{01s} = \frac{2n\cos\phi_0}{n\cos\phi_0 + (n_e^2 - n^2\sin^2\phi_0)^{\frac{1}{2}}}$$
$$t_{12s} = \frac{2(n_e^2 - n^2\sin^2\phi_0)^{\frac{1}{2}}}{n\cos\phi_0 + (n_e^2 - n^2\sin^2\phi_0)^{\frac{1}{2}}}. \tag{7.13}$$

For incident light of wavelength of λ, Eqs. (7.5) and (7.4) can be written as:

$$\tau = f(n_c, n_f, f, n, d, \frac{\Lambda}{\lambda}, \phi) \tag{7.14}$$

$$\rho = f(n_c, n_f, f, n, d, \frac{\Lambda}{\lambda}, \phi) \tag{7.15}$$

To achieve QWR in reflection, the magnitude of the complex reflection coefficients for the p and s polarizations must be equal and the phase shift between them must equal $\frac{\pi}{2}$, i.e.,

$$|\rho| = |\frac{r_p}{r_s}| = 1 \tag{7.16}$$

$$\arg(\rho) = \Delta = \pm 90^o \tag{7.17}$$

Similarly, to achieve QWR in transmission, the magnitude of the complex transmission coefficients for the p and s polarizations must be equal and the phase shift between them

must equal $\frac{\pi}{2}$, equivalently we write:

$$|\tau| = |\frac{t_p}{t_s}| = 1 \tag{7.18}$$

$$\arg(\tau) = \Delta = \pm 90^o \tag{7.19}$$

To achieve 50-50% beam splitter with dual QWR in reflection and transmission, Eqs. (7.16)-(7.19) must be satisfied simultaneously with the following condition:

$$T_p = T_s = R_p = R_s = 0.5 \tag{7.20}$$

7.3 50-50% Beam Splitter with Dual Quarter-Wave Retardation in Reflection and Transmission at 30° Angle of Incidence

A 50-50% beam splitter design with dual QWR is presented at an angle of incidence $\phi = 30^o$, using a 1-D PCL of thickness $d = 2.8843$ μm, coating material of refractive index $n_c = 1.6666$ and filling factor $f = 0.401$. The layer is deposited on an optically isotropic substrate of refractive index $n = 4.0030$ and the gaps between grating ridges are assumed to be filled with isotopic material of refractive index $n_f = 4.0030$ which matches the prism refractive index, $n_f = n$ (see Table 7.1.)

Figure 7.2 shows the intensity reflectance R_s of s polarization and R_p of p polarization as functions of the angle of incidence ϕ, for $28^o \leq \phi \leq 32^o$, with all other parameters kept constant. At the design angle $\phi = 30^o$, we have 50-50% beam splitter for s polarization and p polarization. The intensity reflectance R_s of s polarization is less sensitive to changing the angle of incidence ϕ than the p polarization. The p polarization depends on frustrated total internal reflection (FTR), $\phi_{cp} = 29.1757^o$. Changing the angle of incidence alters FTR for s

Table 7.1: Design parameters for 50-50% beam splitter with dual QWR using $\Lambda/\lambda = 10$.

n_c	n_f	f	n_e	n_o	n	$d(\mu\text{m})$	ϕ	ϕ_{cp}	ϕ_{cs}
1.6666	4.0030	0.401	2.3642	1.9514	4.0030	2.8843	30.0^o	29.1754^o	36.2001^o

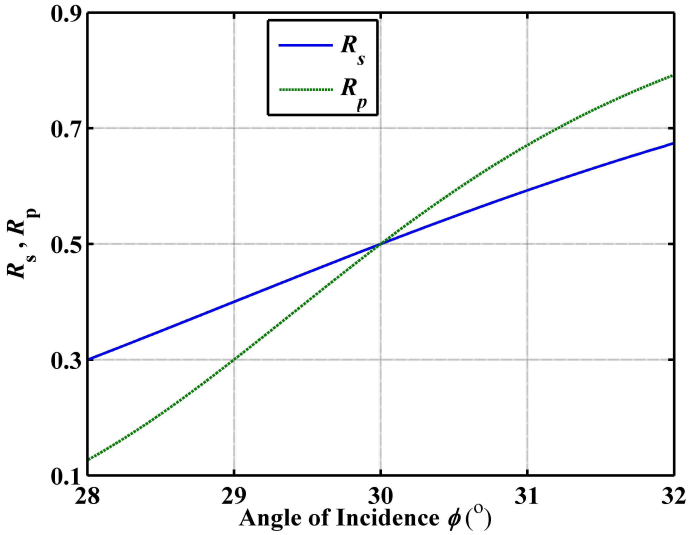

Figure 7.2: Intensity reflectaces R_s of s polarization and R_p of p polarization as functions of the angle of incidence ϕ, with PCL coating $n_c = 1.6666$, PCL thickness $d = 2.8843$ μm, $\frac{\Lambda}{\lambda} = 10$, prism index $n = 4.0030$, and filling factor $f = 0.401$.

polarization. This high sensitivity of intensity reflectances limits the FOV of the splitter.

Figure 7.3 shows retardance $\Delta(\phi)$ in transmission and in reflection as functions of ϕ, for $28^o \leq \phi \leq 32^o$, with all other parameters kept constant. QWR ($\Delta = 90^o$) in reflection and in transmission is achieved at the design angle $\phi = 30^o$.

Figure 7.4 shows the intensity reflectance R_s of s polarization and R_p of p polarization as functions of the filling factor f, for $0.36 \leq f \leq 0.44$, with all other parameters kept constant. The reflectance of the s polarization shows high sensitivity to changes of the filling factor which limits the practical application of the design.

Figure 7.5 shows retardance $\Delta(\phi)$ in transmission and in reflection as a function of the filling factor f, for $0.36 \leq f \leq 0.44$, with all other parameters kept constant. A change of $\approx 10\%$ in the filling factor results in $> 12^o$ deviation from the 90^o phase shift between p and s polarizations, which also limits the practical usefulness of this CPBS design.

Figure 7.6 shows the intensity reflectance R_s of s polarization and R_p of p polarization and Fig 7.7 shows retardance $\Delta(\phi)$ in transmission and in reflection as functions of the layer thickness d, for $2.6 \leq d \leq 3.1$ μm, with all other parameters kept constant. Both figures

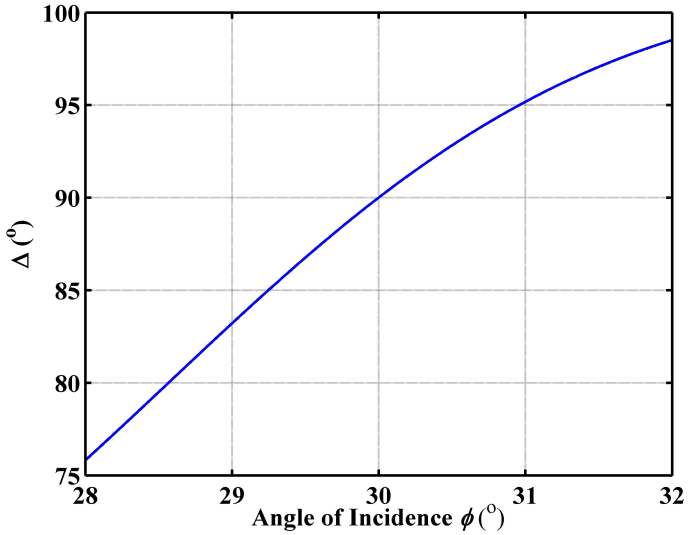

Figure 7.3: Retardance $\Delta(\phi)$ as a function of the angle of incidence ϕ, with PCL coating $n_c = 1.6666$, PCL thickness $d = 2.8843$ μm, $\frac{\Lambda}{\lambda} = 10$, prism index $n = 4.0030$, and filling factor $f = 0.401$.

show less sensitivity to changes of the layer thickness as compared to other parameters.

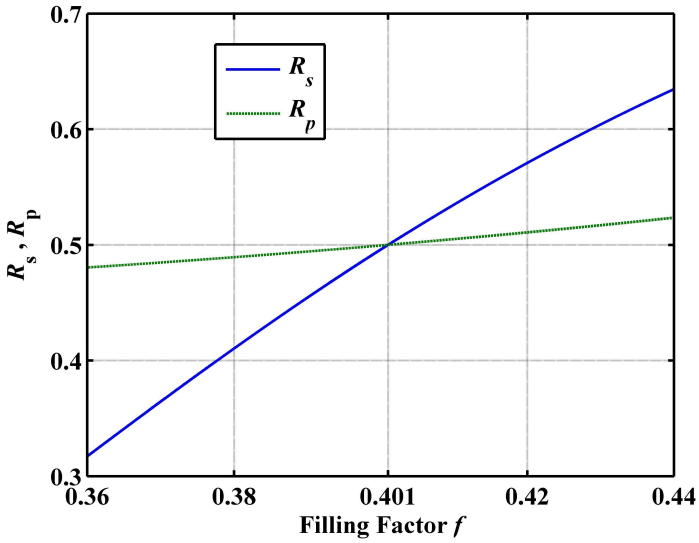

Figure 7.4: Intensity reflectances R_s of s polarization and R_p of p polarization as functions of the filling factor f, with PCL coating $n_c = 1.6666$, PCL thickness $d = 2.8843$ μm, $\frac{\Lambda}{\lambda} = 10$, prism index $n = 4.0030$, and angle of incidence $\phi = 30.0^o$.

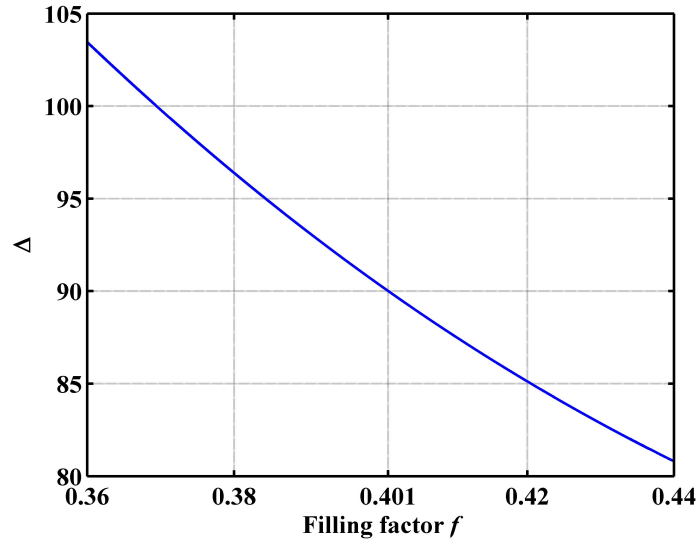

Figure 7.5: Retardance $\Delta(f)$ as a function of the filling factor f, with PCL coating $n_c = 1.6666$, PCL thickness $d = 2.8843$ μm, $\frac{\Lambda}{\lambda} = 10$, prism index $n = 4.0030$, and angle of incidence $\phi = 30.0^o$.

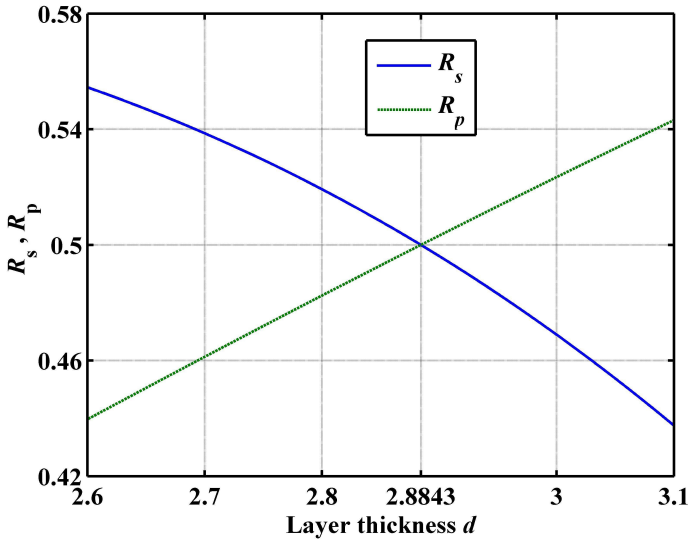

Figure 7.6: Intensity reflectances R_s of s polarization and R_p of p polarization as functions of PCL thickness d, with PCL coating $n_c = 1.6666$, angle of incidence $\phi = 30.0^o$, $\frac{\Lambda}{\lambda} = 10$, prism index $n = 4.0030$, and filling factor $f = 0.401$.

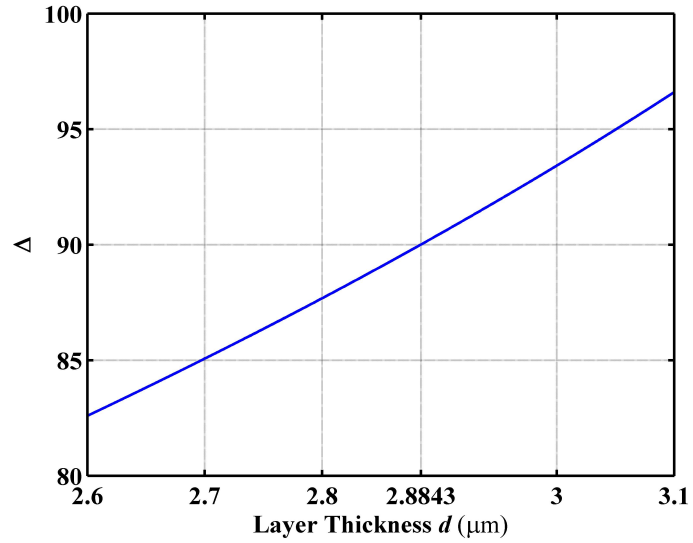

Figure 7.7: Retardance $\Delta(d)$ as a function of PCL thickness d, with PCL coating $n_c = 1.6666$, angle of incidence $\phi = 30.0^o$, $\frac{\Lambda}{\lambda} = 10$, prism index $n = 4.0030$, and filling factor $f = 0.401$.

Chapter 8

Conclusions

Detailed and explicit analysis of the conditions that are required to achieve quarter-wave retardation QWR on TIR at the base of a prism, which is coated with a single-layer optical interference coating, have been presented. For a given prism refractive index and angle of incidence, optimal values of the refractive index and thickness of the coating for QWR are determined. Specific results are presented in Chapter 2 over a range of incidence angles for TIR QWR that use transparent coatings on glass and ZnS substrates. A QWR that uses Si_3N_4-coated N-BK10-Schott glass prism is described with excellent spectral response and retardance error of $< 3^o$ over the 400-600 nm visible range.

PBSs that use SWS 1-D PCL embedded in a high–index cube prism are demonstrated. Such PBSs are based on index matching and total transmission of the p polarization and total internal reflection of the s polarization at the prism-PCL interface at a 45^o angle of incidence, as shown in Chapter 3. Results obtained for two material systems (ZnTe-ZnS and Ge-Si) in Chapters 4 and 5, respectively, show excellent performance over a broad IR spectral range, wide field of view, and insensitivity to small errors of the grating filling factor. Also PBS using the ZnTe-ZnS material system is demonstrated in Chapter 6 for visible spectral ranges showing high-performance parameters .

A 50–50% CPBS using SWS 1-D PCL embedded in a high-index cube prism is presented in Chapter 7. Such CPBSs are sensitive to small changes in design parameters, which limits their practical use.

Bibliography

[1] J. M. Bennett, "Polarization," in Handbook of Optics, M. Bass, E. W. Van Stryland, D. R. Williams, and W. L. Wolfe, eds. (McGraw-Hill, 1995), Vol. I, Chap. 5.

[2] R. M. A. Azzam and N. M. Bashara, *Ellipsometry and Polarized Light* (North-Holland, 1987).

[3] D. A. Holmes, "Exact Theory of Retardation Plates," J. Opt. Soc. Am. 54, 1115-1120 (1964).

[4] R. J. King, "Quarter-wave retardation systems based on the Fresnel rhomb principle," J. Sci. Instrum. 43, 617-622 (1966).

[5] J. M. Bennett, "A Critical Evaluation of Rhomb-Type Quarterwave Retarders," Appl. Opt. 9, 2123-2129 (1970).

[6] I. Filinski and T. Skettrup, "Achromatic phase retarders constructed from right-angle prisms: design," Appl. Opt. 23, 2747-2751 (1984).

[7] A. M. Kanan and R. M. A. Azzam, "In-line quarter-wave retarders for the IR using total refraction and total internal reflection in a prism," Opt. Eng. 33, 2029-2033 (1994).

[8] R. M. A. Azzam and M. M. K. Howlader, "Silicon-based polarization optics for the 1.30 and 1.55 μm communication wavelengths," J. Lightwave Technol. 14, 873-878 (1996).

[9] R. M. A. Azzam and H. K. Khanfar, "Polarization properties of retroreflecting right-angle prisms," Appl. Opt. 47, 359-364 (2008).

[10] R. M. A. Azzam and H. K. Khanfar, "In-line broadband 270^o ($3\lambda/4$) chevron four-reflection wave retarders," Appl. Opt. 47, 4878–4883 (2008).

[11] R. M. A. Azzam, "Phase shifts that accompany total internal reflection at a dielectric-dielectric interface," J. Opt. Soc. Am. A 21, 1559–1563 (2004).

[12] R. M. A. Azzam and C. L. Spinu, "Achromatic angle-insensitive infrared quarter-wave retarder based on total internal reflection at the Si-SiO_2 interface," J. Opt. Soc. Am. A 21, 2019–2022 (2004).

[13] E. Spiller, "Totally reflecting thin-film phase retarders," Appl. Opt. 23, 3544-3549 (1984).

[14] E. Cojocaru, R. Dabu, V. Draganescu, T. Julea, and F. Nichitiu, "Achromatic thin-film totally reflecting quarterwave retarders," Appl. Opt. 28, 211–212 (1989).

[15] R. H. Muller, "Definitions and Conventions in Ellipsometry," Surf. Sci., 16, 14–33, (1969).

[16] T. Bååk, "Silicon oxynitride; a material for GRIN optics," Appl. Opt. 21, 1069–1072 (1982).

[17] Data available at `http://www.cerac.com/pubs/proddata/y2o3.htm`.

[18] M. Debenham, "Refractive indices of zinc sulfide in the 0.405-13-m wavelength range," Appl. Opt. 23, 2238–2239 (1984).

[19] Data available at `http://www.us.schott.com/optics\_devices/english/products/flash/abbediagramm\_flash.html`.

[20] J. D. Joannopoulos, S. G. Johnson, R. D. Meade, and J. N. Winn, *Photonic Crystals: Molding the Flow of Light*, 2^{nd} edition (Princeton Univ. Press, 2008).

[21] P. Lalanne and J. Hugonin, "High-order effective-medium theory of subwavelength gratings in classical mounting: application to volume holograms," J. Opt. Soc. Am. A 15, 1843-1851 (1998).

[22] L. Carretero, M. Ulibarrena, S. Blaya, and A. Fimia, "One-Dimensional Photonic Crystals with an Amplitude-Modulated Dielectric Constant in the Unit Cell," Appl. Opt. 43, 2895-2899 (2004).

[23] P. Szczepanski, T. Osuch, and Z. Jaroszewicz, "Modeling of amplification and light generation in one-dimensional photonic crystal using a multiwavelength transfer matrix approach," Appl. Opt. 48, 5401-5406 (2009).

[24] R. Bräuer and O. Bryngdahl, "Electromagnetic diffraction analysis of two-dimensional gratings," Opt. Commun. 100, 15 (1993).

[25] P. Lalanne, "Effective medium theory applied to photonic crystals composed of cubic or square cylinders," Appl. Opt. 35, 5369–5380 (1996).

[26] H. Kikuta, Y. Ohira, H. Kubo, and K. Iwata, "Effective medium theory of two-dimensional subwavelength gratings in the non-quasi-static limit," J. Opt. Soc. Am. A 15, 1577–1585 (1998).

[27] A. Sharkawy, S. Shi, and D. W. Prather, "Multichannel Wavelength Division Multiplexing with Photonic Crystals," Appl. Opt. 40, 2247–2252 (2001).

[28] W. Yu, T. Konishi, T. Hamamoto, H. Toyota, T. Yotsuya, and Y. Ichioka, "Polarization-Multiplexed Diffractive Optical Elements Fabricated by Subwavelength Structures," Appl. Opt. 41, 96–100 (2002).

[29] G. Lifante, "Effective index method for modelling sub-wavelength two-dimensional periodic structures," Phys. Scrip., T118, 72–77 (2005).

[30] Y. Ono, "Transmittance analysis of three-dimensional photonic crystals by the effective medium theory," Appl. Opt. 45, 131–136 (2006).

[31] Y. Liu, S. Liu, and X. Zhang, "Fabrication of three-dimensional photonic crystals with two-beam holographic lithography," Appl. Opt. 45, 480–483 (2006).

[32] A. Dwivedi, J. Xavier, J. Joseph, and K. Singh, "Formation of all fourteen Bravais lattices of three-dimensional photonic crystal structures by a dual beam multiple-exposure holographic technique," Appl. Opt. 47, 1973–1980 (2008).

[33] C. Chen, H. Chien, and P. Luan, "Photonic Crystal Beam Splitters," Appl. Opt. 43, 6187–6190 (2004).

[34] E. Schonbrun, Q. Wu, W. Park, T. Yamashita, and C. J. Summers, "Polarization beam splitter based on a photonic crystal heterostructure," Opt. Lett. 31, 3104–3106 (2006).

[35] J. She, E. Forsberg, X. Y. Ao, S. L. He"High-efficiency polarization beam splitters based on a two-dimensional polymer photonic crystal," J. Opt. A: Pure Appl. Opt. 8, 345–349 (2006).

[36] V. Zabelin, L. A. Dunbar, N. Le Thomas, R. Houdr, M. V. Kotlyar, L. O'Faolain, and T. F. Krauss, "Self-collimating photonic crystal polarization beam splitter," Opt. Lett. 32, 530–532 (2007).

[37] O. Kilic, S. Fan, and O. Solgaard, "Analysis of guidedresonance-based polarization beam splitting in photonic crystal slabs," J. Opt. Soc. Am. A 25, 2680-2692 (2008).

[38] R. M. A. Azzam, "Division–of–amplitude photopolarimeter (DOAP) for the simultaneous measurement of all four Stokes parameters of light," Opt. Acta 29, 685-689 (1982).

[39] C–H. Lee, Y. Chiu, and H–P. D. Shieh, "High-extinction-ratio micro polarizing beam splitter for short wavelength optical storage applications," Opt. Express 13, 10292-10301 (2005).

[40] D. R. Solli, C. F. McCormick, R. Y. Chiao, and J. M. Hickman,"Photonic crystal polarizers and polarizing beam splitters," J. Appl. Phys. 93, 9429-9431 (2003).

[41] D. Mao, Z. Ouyang, J. Wang, C. Liu, and C. Wu, "A photonic-crystal polarizer integrated with the functions of narrow bandpass and narrow transmission-angle filtering," Appl. Phys. B 90, 127-131 (2008).

[42] C. W. Haggans, L. Li, T. Fujita, and R. Kostuk, "Lamellar gratings as polarization components for specularly reflected beams, J. Mod. Opt. 40, 675-686 (1993).

[43] J. Ma and M. L. Povinelli, "Large tuning of birefringence in two strip silicon waveguides via optomechanical motion," Opt. Express 17, 17818–17828 (2009).

[44] D. L. Brundrett, E. N. Glytsis, and T. K. Gaylord, "Subwavelength transmission grating retarders for use at 10.6 m," Appl. Opt. 35, 6195–6202 (1996).

[45] D. R. Solli, C. F.McCormick, R. Y. Chiao, and J.M. Hickmann, "Birefringence in two-dimensional bulk photonic crystals applied to the construction of quarter waveplates," Opt. Express 11, 125–133 (2003).

[46] D.-E. Yi, Y.-B. Yan, H.-T. Liu, Si-Lu, and G.-F. Jin, "Broadband achromatic phase retarder by subwavelength grating," Opt. Commun. 227, 49-55 (2003).

[47] H. Lim, F. . Ilday, and F. W. Wise, "Femtosecond ytterbium fiber laser with photonic crystal fiber for dispersion control," Opt. Express 10, 1497–1502 (2002).

[48] H. Zhang, S. Li, C. Wah Leung, and H. Lai Wa Chan, "All wavelengths and directions hybrid-guidance photonic crystal fiber and its property of Bragg grating resonance," Appl. Opt. 48, 2468–2472 (2009)

[49] I. V. Fedotov, A. B. Fedotov, L. V. Doronina, and A. M. Zheltikov, "Enhancement of guided-wave two-photon-excited luminescence response with a photonic-crystal fiber," Appl. Opt. 48, 5274–5279 (2009).

[50] M. E. Motamedi, W. H. Southwell, and W. J. Gunning, "Antireflection surfaces in silicon using binary optics technology," Appl. Opt. 31, 4371–4376 (1992).

[51] D. H. Raguin and G. M. Morris, "Antireflection structured surfaces for the infrared spectral region," Appl. Opt. 32, 1154–1167 (1993).

[52] J. Ushida, M. Tokushima, M. Shirane, and H. Yamada, "Systematic design of antireflection coating for semiinfinite one-dimensional photonic crystals using Bloch wave expansion," Appl. Phys. Lett. 82, 7-9 (2003).

[53] S.-G. Lee, J.-S. Choi, J.-E. Kim, H. Y. Park, and C.-S. Kee, "Reflection minimization at two-dimensional photonic crystal interfaces," Opt. Express 16, 4270–4277 (2008).

[54] H. A. Macleod, *Thin Film Optical Filters*, 2nd ed. (McGraw- Hill, 1986).

[55] J. Mouchart, J. Begel, and E. Duda, "Modified MacNeille cube polarizer for a wide angular field," Appl. Opt. 28, 2847-2853 (1989).

[56] L. Li and J. A. Dobrowolski, "Visible broadband, wide-angle, thin-film multilayer polarizing beam splitter," Appl. Opt. 35, 2221-2225 (1996).

[57] L. Li and J. A. Dobrowolski, "High-performance thin film polarizing beam splitter operating at angles greater than the critical angle," Appl. Opt. 39, 2754-2771 (2000).

[58] S. R. Perla and R. M. A. Azzam, "Wide-angle, high-extinctionratio, infrared polarizing beam splitters using frustrated total internal reflection by an embedded centrosymmetric multilayer," Appl. Opt. 46, 4604-4612 (2007).

[59] H. Haidner, P. Kipfer, J. T. Sheridan, J. Schwider, N. Streibl, J. Lindolf, M. Collischon, A. Lang, and J. Hutfless, "Polarizing reflection grating beamsplitter for the 10:6 μm wavelength," Opt. Eng. 32, 1860-1865 (1993).

[60] A. G. Lopez and H. G. Craighead, "Wave-plate polarizing beam splitter based on form-birefringent multilayer grating," Opt. Lett. 23, 1627-1629 (1998).

[61] L. Pajewski, R. Borghi, G. Schettini, F. Frezza, and M. Santarsiero, "Design of a Binary Grating with Subwavelength Features that Acts as a Polarizing Beam Splitter," Appl. Opt. 40, 5898–5905 (2001)

[62] J. Zheng, C. Zhou, J. Feng, and B. Wang, "Polarizing beam splitter of deep-etched triangular-groove fused-silica gratings," Opt. Lett. 33, 1554-1556 (2008).

[63] J. Feng, C. Zhou, B. Wang, and J. Zheng, "Deep silicon grating as high-extinction-ratio polarizing beam splitter," Chin. Opt. Lett. 7, 325-328 (2009).

[64] J. A. Davis, J. Adachi, C. R. Fernndez-Pousa, and I. Moreno, "Polarization beam splitters using polarization diffraction gratings," Opt. Lett. 26, 587–589 (2001).

[65] R. M. A. Azzam and F. A. Mahmoud, "Symmetrically Coated Pellicle Beam Splitters for Dual Quarter-Wave Retardation in Reflection and Transmission," Appl. Opt. 41, 235-238 (2002).

[66] R. M. A. Azzam and A. De, "Circular polarization beam splitter that uses frustrated total internal reflection by an embedded symmetric achiral multilayer coating," Opt. Lett. 28, 355–357 (2003).

[67] R. M. A. Azzam and C. L. Spinu, "Linear-to-circular polarization transformation upon optical tunneling through an embedded low-index film," Opt. Lett. 30, 3183–3185 (2005).

[68] O. Kilic, S. Fan, and O. Solgaard, "Dual Quarter-Wave Retardation Based Polarization Beam Splitting in Photonic Crystal Slabs," in *Photonic Metamaterials: From Random to Periodic*, Technical Dgest (CD) (Optical Society of America, 2006), paper ThD1.

[69] D. L. Brundrett, E. N. Glytsis, and T. K. Gaylord, "Homogeneous layer models for high-spatial-frequency dielectric surface-relief gratings: conical diffraction and antireflection designs," Appl. Opt. 33, 2695-2706 (1994).

[70] W. J. Tropf, M. E. Thomas, and T. J. Harris, "Properties of crystals and glasses," in *Handbook of Optics*, Vol. II, M. Bass, E. W. Van Stryland, D. R. Williams, and W. L. Wolfe, eds. (McGraw-Hill, 1995), Chap. 33.

VITA

Hazem Khanfar was born in Hebron, Palestine in 1977. He received his B.Sc. in Electronics Engineering from Al-Quds University, Jerusalem, Palestine, in 2000 and the M.Sc. in Telecommunication Engineering from Jordan University for Science and Technology, Irbid, Jordan, 2003. He worked as an instructor of electronics at Palestine Polytechnic University, Hebron, Palestine, 2004–2006. Also, he worked as a Teaching Assistant at the Department of Electrical Engineering, 2007–2008, and as a Research Assistant at the Department of Physics, University of New Orleans, 2008-2009, while pursuing his PhD degree. His research interests include Photonic Crystals, Optical Coatings Design, Image and Signal Processing, and Quantum-Dot Lasers.